Seipin and Nem1 establish discrete ER subdomains to initiate yeast lipid droplet biogenesis

Vineet Choudhary[1] , Ola El Atab[1], Giulia Mizzon[2] , William A. Prinz[3] , and Roger Schneiter[1]

Lipid droplets (LDs) are fat storage organelles that originate from the endoplasmic reticulum (ER). Relatively little is known about how sites of LD formation are selected and which proteins/lipids are necessary for the process. Here, we show that LDs induced by the yeast triacylglycerol (TAG)-synthases Lro1 and Dga1 are formed at discrete ER subdomains defined by seipin (Fld1), and a regulator of diacylglycerol (DAG) production, Nem1. Fld1 and Nem1 colocalize to ER–LD contact sites. We find that Fld1 and Nem1 localize to ER subdomains independently of each other and of LDs, but both are required for the subdomains to recruit the TAG-synthases and additional LD biogenesis factors: Yft2, Pex30, Pet10, and Erg6. These subdomains become enriched in DAG. We conclude that Fld1 and Nem1 are both necessary to recruit proteins to ER subdomains where LD biogenesis occurs.

Introduction

Lipid droplets (LDs) are evolutionary conserved fat storage organelles having a multitude of functions (Olzmann and Carvalho, 2019; Walther et al., 2017). The core of LDs is comprised of neutral lipids, typically triacylglycerol (TAG) and steryl esters (SEs), and is enveloped by a phospholipid monolayer. The LD periphery is decorated by structural proteins, such as perilipins, and harbors different lipid metabolic enzymes including acyltransferases and lipases. LDs are formed from the ER where neutral lipid–synthesizing enzymes are located. Upon synthesis, TAG/SEs accumulate between the leaflets of the ER membrane, and they coalesce into lenslike structures that emerge toward the cytosol as they grow, while remaining connected to the ER. Accumulating evidence suggests that LD formation occurs at specific sites in the ER (Adeyo et al., 2011; Chung et al., 2019; Jacquier et al., 2011; Joshi et al., 2018; Kassan et al., 2013; Salo et al., 2019; Wang et al., 2016, 2018). However, relatively little is known about the molecular mechanisms that control LD formation at these sites and which proteins/lipids are necessary for the process.

Proteins implicated in LD formation include seipin (Szymanski et al., 2007), lipin (Pah1; Adeyo et al., 2011), fat storage–inducing transmembrane protein (FIT2; Gross et al., 2011; Kadereit et al., 2008), and Pex30 (Joshi et al., 2018; Wang et al., 2018). Seipin (BSCL2 in humans and Fld1 in yeast) is an ER membrane protein that localizes to ER–LD contact sites

and plays a crucial role in LD formation and adipogenesis (Fei et al., 2008; Salo et al., 2016; Szymanski et al., 2007; Wang et al., 2016). Mutations in human seipin result in loss of fat deposition in adipocytes, a hallmark feature of Berardinelli–Seip congenital lipodystrophy type 2. Seipin facilitates maturation of nascent LDs (Wang et al., 2016) and plays a key role in TAG partitioning between small and large LDs (Salo et al., 2019). Lipin (Pah1 in yeast) encodes a phosphatidate phosphatase that dephosphorylates phosphatidic acid to generate diacylglycerol (DAG). DAG is used by the acyltransferases Lro1 and Dga1 to synthesize TAG and thereby promote LD biogenesis in the ER (Adeyo et al., 2011; Barbosa et al., 2015; Karanasios et al., 2013). Deletion of Pah1 or Fld1 attenuates LD biogenesis, resulting in the accumulation of neutral lipids in the ER (Adeyo et al., 2011; Cartwright et al., 2015). FIT2, another ER membrane protein, is expressed in all cell types, widely conserved, and plays a crucial role in LD formation. Lack of FIT2 is lethal in higher eukaryotes (Choudhary et al., 2015; Goh et al., 2015). Budding yeast has two homologues of FIT2, Yft2 and Scs3. FIT2 proteins bind DAG and TAG in vitro (Gross et al., 2011), and defects in FIT2 result in aberrant emergence of LDs from the ER and the accumulation of DAG (Choudhary et al., 2015, 2018). Recently, we have shown that Yft2 becomes enriched at LD biogenesis sites colocalizes with Nem1 and Fld1 and shows coenrichment with DAG (Choudhary et al., 2018). Two recent studies

[1]Department of Biology, University of Fribourg, Fribourg, Switzerland; [2]Electron Microscopy Core Facility, European Molecular Biology Laboratory, Heidelberg, Germany; [3]National Institute of Diabetes and Digestive and Kidney Diseases, National Institutes of Health, Bethesda, MD.

Correspondence to Vineet Choudhary: vchoudhary@aiims.edu;   Roger Schneiter: roger.schneiter@unifr.ch;   V. Choudhary's present address is All India Institute of Medical Sciences, Department of Biotechnology, New Delhi, India.

identified Pex30, a yeast protein having an N-terminal reticulon homology domain that tubulates subdomains of the ER to mark ER sites at which LDs and preperoxisomal vesicles originate (Joshi et al., 2018; Wang et al., 2018). Lack of Pex30 results in a significant delay in LD formation and defects in peroxisome biogenesis (Joshi et al., 2018; Wang et al., 2018).

In this study, we show that LDs are formed from discrete ER subdomains. These sites are stable and are defined by Fld1 and Nem1. We demonstrate that the localization of Fld1 and Nem1 at these specialized ER subdomains is independent of each other, or the presence of neutral lipids, and that both are required together to create functional sites of LD biogenesis.

Results

sLro1 localizes to sites of LD biogenesis in the ER

To visualize the earliest stages of LD biogenesis, we used a *Saccharomyces cerevisiae* strain in which LD formation can be induced de novo. Production of neutral lipids in yeast is controlled by four enzymes: Are1 and Are2 catalyze SE production, whereas Dga1 and Lro1 synthesize TAG. Cells missing all four proteins *are1Δ are2Δ dga1Δ lro1Δ* (hereafter 4ΔKO) lack the capacity to produce neutral lipids and hence have no detectable LDs (Sandager et al., 2002). All four proteins are ER localized except for Dga1, which shows dual localization, in the ER as well as on LDs (Sorger and Daum, 2002). Expression of any one of the four enzymes is sufficient to induce LD formation (Sandager et al., 2002). Lro1, an orthologue of mammalian lecithin cholesterol acyltransferase, has a small cytoplasmic domain, a transmembrane domain (TMD), and a large ER luminal domain containing the conserved active site residues (Fig. 1 A; Choudhary et al., 2011).

To investigate whether the soluble domain of Lro1 can catalyze TAG formation when expressed in the cytoplasm, we fused this domain of Lro1 (aa 98–661) to GFP and two phenylalanines in an acidic tract (FFAT) motifs, which bind to the ER-resident protein Scs2 (Loewen et al., 2003), and to the purification tag maltose-binding protein (MBP; Fig. 1 B). Scs2 is the yeast homologue of mammalian vesicle-associated membrane protein–associated proteins, which are enriched at membrane contact sites (Wu et al., 2018). The fusion protein called GFP-FFAT-sLro1 was expressed on a plasmid under a galactose-inducible promoter in 4ΔKO cells. Galactose induction of GFP-FFAT-sLro1 resulted in rapid production of TAG to levels that are similar to those observed for native Lro1, as monitored by radiolabeling cells with [³H]palmitic acid (Fig. 1, C and D). This indicates that GFP-FFAT-sLro1 is catalytically active and can synthesize TAG in the cytoplasmic leaflet of the ER membrane.

Next, we monitored the subcellular localization of GFP-FFAT-sLro1 in 4ΔKO cells, coexpressing the LD marker Erg6-mCherry (Fig. 1 E). Erg6 localizes to the ER in 4ΔKO cells but becomes enriched on LDs as they begin to form (Jacquier et al., 2011). Upon induction in galactose-containing media, GFP-FFAT-sLro1 displayed punctate localization, possibly at sites of nascent LD biogenesis, long before these sites were stained with Erg6-mCherry (Fig. 1 E). By 2 h of galactose induction, ~80% of GFP-FFAT-sLro1 punctae colocalized with Erg6-mCherry

(Fig. 1 F). Induction of GFP-FFAT-sLro1 resulted in a time-dependent increase in protein levels as revealed by Western blot analysis (Fig. 1 G). GFP fused to the FFAT motif alone, on the other hand, did not localize to sites of LD formation, or catalyze TAG formation (Fig. 1, D and F). Replacing the FFAT motif with the transmembrane segment of Sec63 (TMDs 1–3, aa 1–250) resulted in the same punctuate localization of the fusion Sec63(1–250)-GFP-sLro1 as observed for the FFAT containing sLro1, indicating that the punctuate localization is not due to the presence of the FFAT motif (Fig. S1, A and B). When induced in WT cells, GFP-FFAT-sLro1 localized to ER–LD contact sites and partially colocalized with Erg6-mCherry–marked LDs (Fig. S1 C). To determine whether sLro1 punctae correspond to sites of LD biogenesis in the ER, we performed correlative light and electron microscopy (CLEM) imaging on 4ΔKO cells. GFP-FFAT-sLro1 localized to punctate in the ER by fluorescence imaging, and these punctae correlated with electron-translucent LDs in the EM sections (Fig. 1 I). Taken together, these findings indicate that GFP-FFAT-sLro1 localizes to discrete sites in the ER where LDs form, suggesting that TAG synthesis is localized to specialized domains in the ER.

TAG-synthase needs to be ER membrane anchored to produce LDs

We next asked whether the TAG-synthase sLro1 needs to be proximal to a membrane to catalyze TAG synthesis and drive LD biogenesis. Therefore, we generated two fusion constructs of sLro1, one to express it in the cytosol and a second to express it in the ER lumen without being anchored to the ER membrane (Fig. S1, D and E). Therefore, sLro1(aa 98–661) was fused to GFP (GFP-sLro1) or to the signal sequence of Kar2 and a HDEL retention signal (ssKar2-GFP-sLro1-HDEL). 4ΔKO cells expressing GFP-sLro1 and ssKar2-GFP-sLro1-HDEL from a galactose-inducible promoter failed to produce LDs or to catalyze any detectable TAG (Fig. S1, F and G). These findings indicate that TAG synthesis by sLro1 in vivo requires ER membrane proximal localization of the enzyme.

Fld1 and Nem1 localize to discrete ER subdomains even in the absence of LDs

We investigated how GFP-FFAT-sLro1 becomes enriched at discreate sites in the ER. In yeast, mature LDs mostly remain connected to the ER (Jacquier et al., 2011). Two ER proteins, Nem1 and Fld1, are known to be associated with sites of LD biogenesis (Szymanski et al., 2007). Nem1 is part of a phosphatase complex, Nem1-Spo7, that activates phosphatidic acid phosphatase (Pah1), the yeast homologue of mammalian lipin, to regulate DAG formation, an important precursor for TAG synthesis (Fig. S2 A; Pascual and Carman, 2013). Nem1 shows punctate localization at ER sites that are in proximity to LDs, and cells lacking Nem1 have reduced numbers of LDs, and they accumulate the neutral lipid dye BODIPY in the ER membrane (Adeyo et al., 2011). In agreement with this, we found that the number of Erg6-mCherry–marked LDs was strongly reduced in cells lacking Nem1 (*nem1Δ*), Spo7 (*spo7Δ*), or Pah1 (*pah1Δ*), and these cells displayed accumulation of BODIPY throughout the ER membrane (Fig. S2 B). Like Nem1, Fld1 also localizes at ER–LD
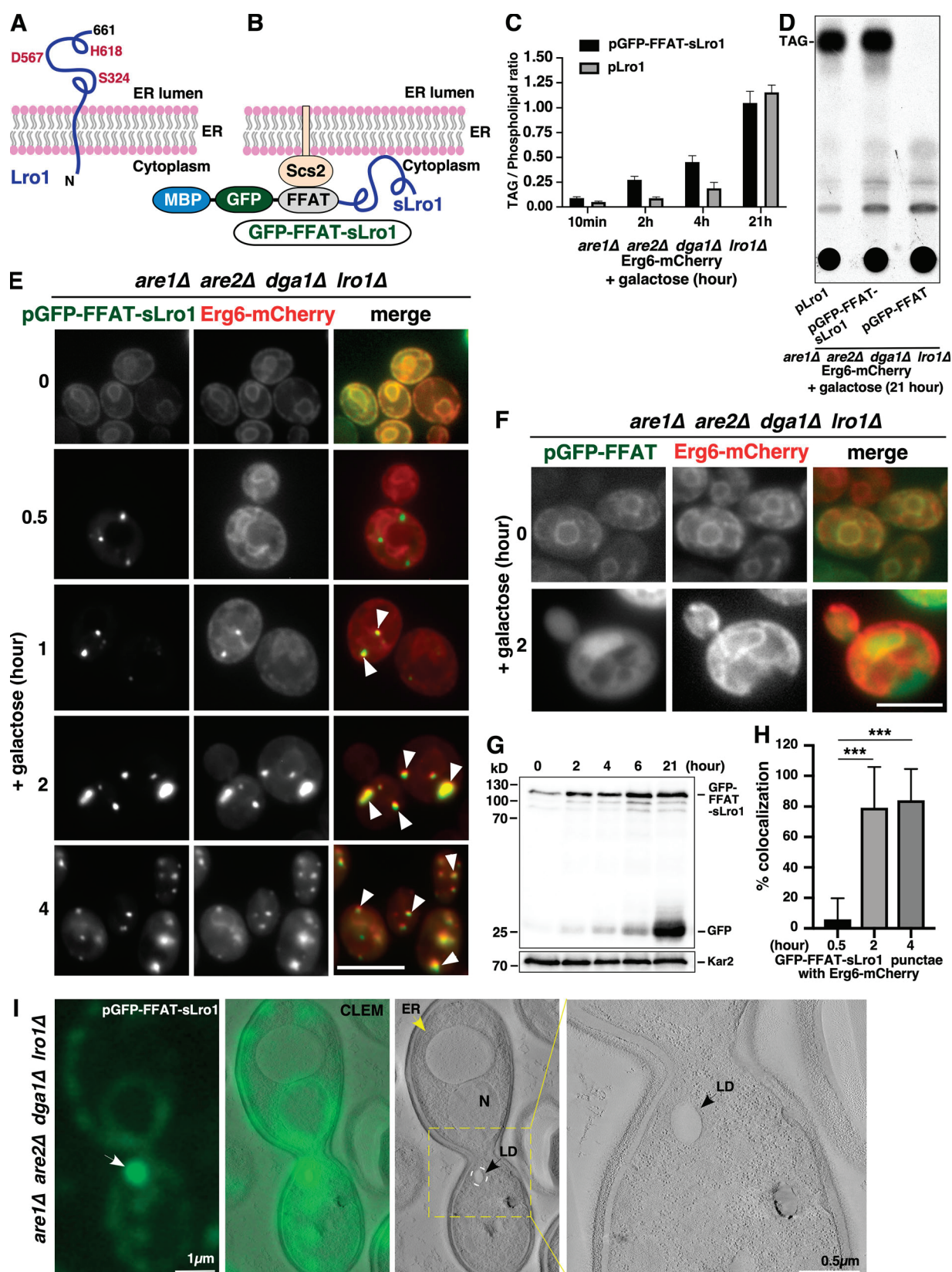
2

Figure 1. **The TAG-synthase Lro1 reveals sites of nascent LD biogenesis in the ER. (A)** Topology of TAG-synthase Lro1. N, nucleus. **(B)** Design of the MBP-GFP-FFAT-sLro1 chimera, which binds the ER-resident Scs2 through a FFAT motif and has its catalytic domain exposed to the cytoplasm. **(C and D)** GFP-FFAT-sLro1 is enzymatically active. Cells of indicated genotypes were grown in SC raffinose media, diluted in SC galactose containing [³H]palmitic acid, and grown for the indicated period of time. Lipids were extracted and separated by TLC. TAG-to-phospholipids ratio is plotted in C, and TLC image of 21-h time point is shown in D. Data represent mean ± SD of three independent experiments. **(E and F)** GFP-FFAT-sLro1 localizes to discrete ER subdomains. 4ΔKO cells expressing

3

genomic Erg6-mCherry and coexpressing GFP-FFAT-sLro1 (E) or GFP-FFAT (F) from a galactose-inducible promoter. Arrowheads indicate colocalization between GFP-FFAT-sLro1 and Erg6-mCherry. Scale bar, 5 μm. **(G)** Western blot showing expression of GFP-FFAT-sLro1 or Kar2 after galactose induction for the indicated period of time. **(H)** Quantification of colocalization between GFP-FFAT-sLro1 and Erg6-mCherry. Percentage of GFP-FFAT-sLro1 puncta that colocalize with Erg6-mCherry after galactose induction. Data represent mean ± SD, $n > 50$ cells; ***, $P < 0.0005$. **(I)** GFP-FFAT-sLro1 colocalizes with LDs. CLEM imaging of 4ΔKO cells expressing GFP-FFAT-sLro1. Cells were induced in galactose for 1 h. GFP-FFAT-sLro1 is enriched at a discrete site in the ER by fluorescence imaging and colocalizes with an electron-translucent LD by EM. Yellow arrow demarcates ER, white arrow denotes GFP-FFAT-sLro1 puncta, and black arrow denotes an LD. N, nucleus.

contact sites and plays an important role in maturation of LDs (Fei et al., 2008; Szymanski et al., 2007). Cells lacking Fld1 accumulate many small LDs and a few supersized LDs that are up to 30 times the size of a typical WT LD, a phenotype that we confirm (Fig. S2 C). Surprisingly, some of the BODIPY-stained supersized LDs in *fld1Δ* cells failed to colocalize with Erg6-mCherry (Fig. S2 C). Unlike *nem1Δ*, *spo7Δ*, *pah1Δ*, or *fld1Δ* mutants, WT cells do not tend to accumulate neutral lipids in the ER, and LDs appear homogenous in size, as evidenced by similarly sized, BODIPY-stained LDs that colocalized with Erg6-mCherry (Fig. S2 D). These findings suggest that the Pah1-regulating Nem1 complex and Fld1 play a role in determining the number or distribution of sites of LD biogenesis. We wondered whether the Nem1 complex plays a role in LD biogenesis that is independent of its regulation of Pah1. To test this, we expressed a constitutively active version of Pah1, called Pah1-7P, that does not require activation by Nem1-Spo7 (O'Hara et al., 2006). Cells lacking Nem1, Spo7, or Pah1 and expressing Pah1-7P showed no accumulation of BODIPY in the ER and had LDs that were similar to those observed in WT (Fig. S2 E).

To investigate the role of Fld1 and Nem1 in determining sites of LD biogenesis, we visualized their localization in 4ΔKO cells. Surprisingly, Fld1-mCherry and Nem1-mCherry showed punctate ER localization in 4ΔKO cells lacking any detectable BODIPY-stained LDs (Fig. S3 A), indicating that the localization of Fld1 and Nem1 to discrete ER sites is independent of neutral lipid synthesis, or the presence of LDs. Next, we investigated whether these Fld1- and Nem1-marked foci are stable over time. Using LiveDrop, a probe to visualize nascent LDs, seipin punctae have previously been shown to move rapidly along the ER and to stably associate LD precursors (Wang et al., 2016). More recently, seipin foci have been shown to lose mobility upon recruitment of LD markers LD540, LiveDrop, or the acyl-coA synthetase ligase 3 (ACSL3), suggesting a role of seipin in defining or stabilizing sites of LD formation (Salo et al., 2019). We visualized the mobility of Fld1-GFP and Nem1-GFP in 4ΔKO cells by time-lapse microscopy. Some of the Fld1-GFP puncta showed rapid mobility, whereas other foci showed slow mobility (Fig. S3 B and Video 1), in agreement with previous observations (Salo et al., 2016, 2019; Wang et al., 2016). However, most of the Nem1-GFP punctae were stable over time (Fig. S3 C and Video 2). Overall, these data suggest that Fld1 and Nem1 localize to ER sites independent of neutral lipid synthesis and that they likely define the location and number of potential LD biogenesis sites.

Fld1 and Nem1 define ER subdomains that recruit the TAG-synthase

Given that the localization of Fld1 and Nem1 is independent of the presence of LDs, we wondered whether GFP-FFAT-sLro1

punctae observed upon induction (Fig. 1 D) colocalize with Fld1 or Nem1. To localize sites of TAG synthesis, we induced GFP-FFAT-sLro1 in 4ΔKO cells coexpressing Fld1-mCherry or Nem1-mCherry. Fld1-mCherry and Nem1-mCherry showed punctate ER localization in cells lacking LDs (Fig. 2, A and B; 0-h time point). Upon induction, GFP-FFAT-sLro1 specifically localized to spots marked by Fld1-mCherry or Nem1-mCherry (Fig. 2, A and B; 1-h time point). After 1 h of induction, ~80% of Fld1-mCherry (Fig. 2, C and D) or Nem1-mCherry (Fig. 2, E and F) punctae colocalized with GFP-FFAT-sLro1. This suggests that GFP-FFAT-sLro1 specifically localizes to sites where Fld1 or Nem1 reside, suggesting that TAG is synthesized at these discrete ER subdomains. However, in the absence of either Fld1, Nem1, or Pah1, GFP-FFAT-sLro1 failed to get recruited at these sites and instead was localized throughout the ER, suggesting that TAG is produced ectopically (Fig. 2 G). This is consistent with the reported accumulation of TAG in the ER of *fld1Δ*, *nem1Δ*, and *pah1Δ* mutants (Adeyo et al., 2011; Cartwright et al., 2015). Overexpression of Fld1-mCherry in *fld1Δ* cells resulted in functional ER sites that recruited GFP-FFAT-sLro1 (Fig. 2 H and Video 3). Overall, these data indicate that ER subdomains enriched in seipin or Nem1 recruit GFP-FFAT-sLro1 to facilitate localized TAG synthesis and hence drive LD formation (Fig. 2 I).

Fld1 and Nem1 recruit native Lro1

We next asked whether native Lro1 would also localize to Fld1- or Nem1-marked ER sites. Therefore, we generated GFP-tagged, full-length Lro1 (GFP-Lro1) and expressed it from a galactose-inducible promoter. Induction of GFP-Lro1 in 4ΔKO cells coexpressing genomic Fld1-mCherry or Nem1-mCherry resulted in colocalization with Fld1 (Fig. 3, A and C; 1-h time point) or Nem1 (Fig. 3, B and E; 1-h time point), although GFP-Lro1 did not become as enriched in puncta as GFP-FFAT-sLro1. Upon 1 h of induction, ~60% of Fld1-mCherry and ~70% of Nem1-mCherry punctae associated with GFP-Lro1 (Fig. 3 D). In cells lacking either Fld1, Nem1, or Pah1, GFP-Lro1 remained uniformly distributed throughout the ER (Fig. 3 F), consistent with ectopic formation of TAG in the ER of these mutants (Adeyo et al., 2011; Cartwright et al., 2015).

To investigate how Fld1 and Nem1 organize sites of LD biogenesis, we first examined whether these two proteins colocalize. Therefore, WT cells expressing Nem1-GFP and coexpressing Fld1-mCherry from a plasmid were analyzed by fluorescence microscopy. Nem1-GFP showed strong colocalization with Fld1-mCherry (Fig. S3 D). Approximately 97% of Nem1-GFP punctae colocalized with Fld1-mCherry, whereas ~33% of Fld1-mCherry was associated with Nem1-GFP (Fig. S3 E). We wondered whether colocalization between Nem1 and Fld1 increases upon induction of LD biogenesis. Therefore,
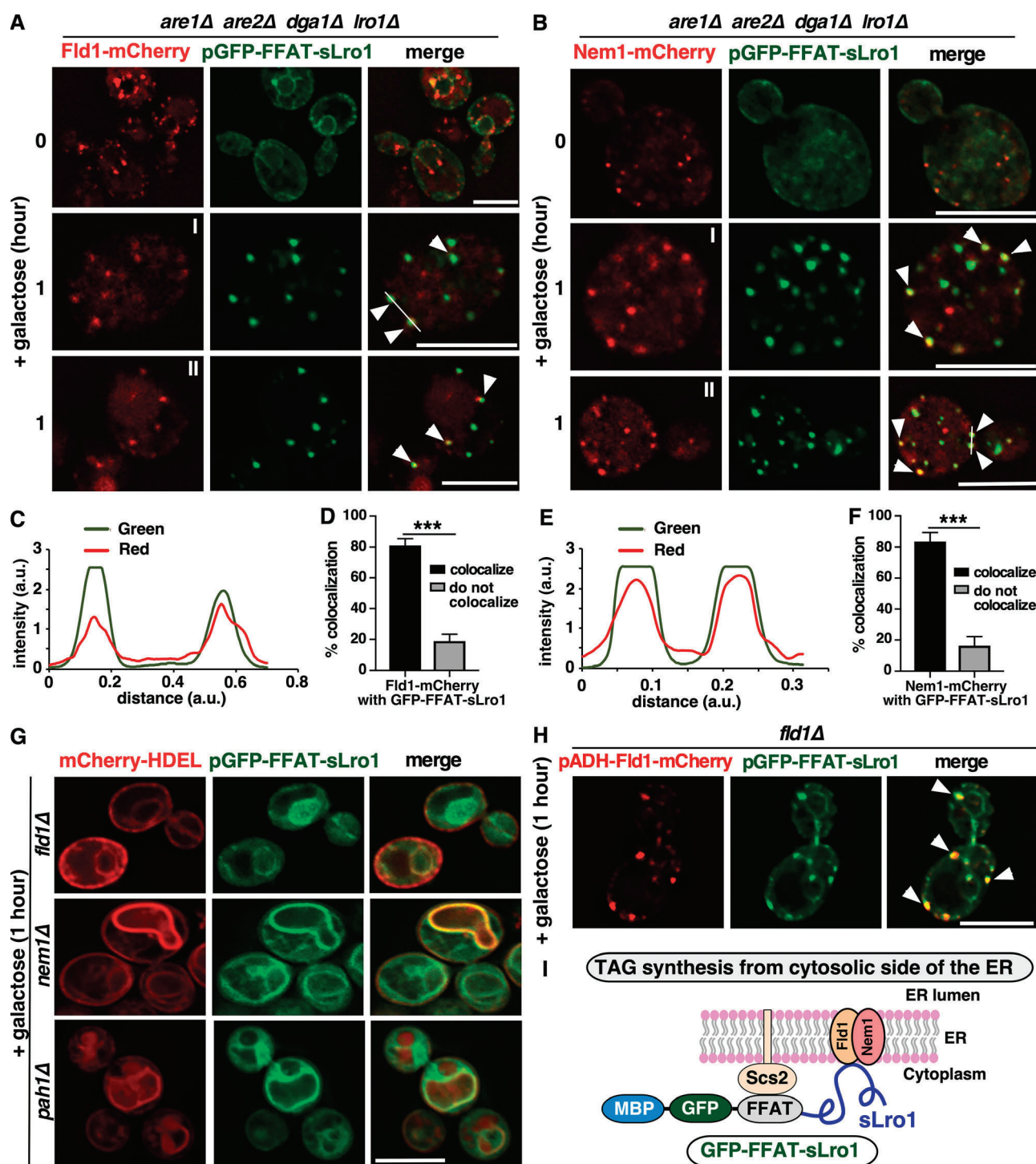
Figure 2. Fld1 and Nem1 define ER subdomains for the recruitment of the TAG-synthase. (A and B) 4ΔKO cells expressing Fld1-mCherry (A) or Nem1-mCherry (B) together with GFP-FFAT-sLro1 from a galactose-inducible promoter. Fld1-mCherry (A) and Nem1-mCherry (B) show punctate localization in the absence of LDs (0 h). Upon 1 h of induction, GFP-FFAT-sLro1 colocalizes with Fld1-mCherry (A) or Nem1-mCherry (B). White arrowheads indicate colocalization of sLro1 with Fld1 (A) and Nem1 (B), respectively. Two examples of the 1 h time points are shown (I, II) for A and B. Scale bars, 5 μm. **(C and E)** Line scan of signal intensity along the white line shown in A (I) and B (II), respectively. **(D and F)** Quantification of colocalization between Fld1 (D) and Nem1 (F) punctae with sLro1. Data are means ± SD, *n* > 50 cells; ***, P < 0.0005. **(G)** Fld1, Nem1, and Pah1 are required to recruit the TAG-synthase into discrete ER foci. Cells lacking Fld1, Nem1, or Pah1 expressing GFP-FFAT-sLro1 and coexpressing mCherry-HDEL to mark the ER. Scale bar, 5 μm. **(H)** Overexpression of Fld1 in *fld1Δ* cells creates ER sites that recruit GFP-FFAT-sLro1. Fluorescence microscopy of *fld1Δ* cells harboring Fld1-mCherry and coexpressing GFP-FFAT-sLro1. White arrowheads denote colocalization between Fld1 and sLro1. Scale bar, 5 μm. **(I)** Cartoon showing the recruitment of sLro1 at Fld1 and Nem1 sites.
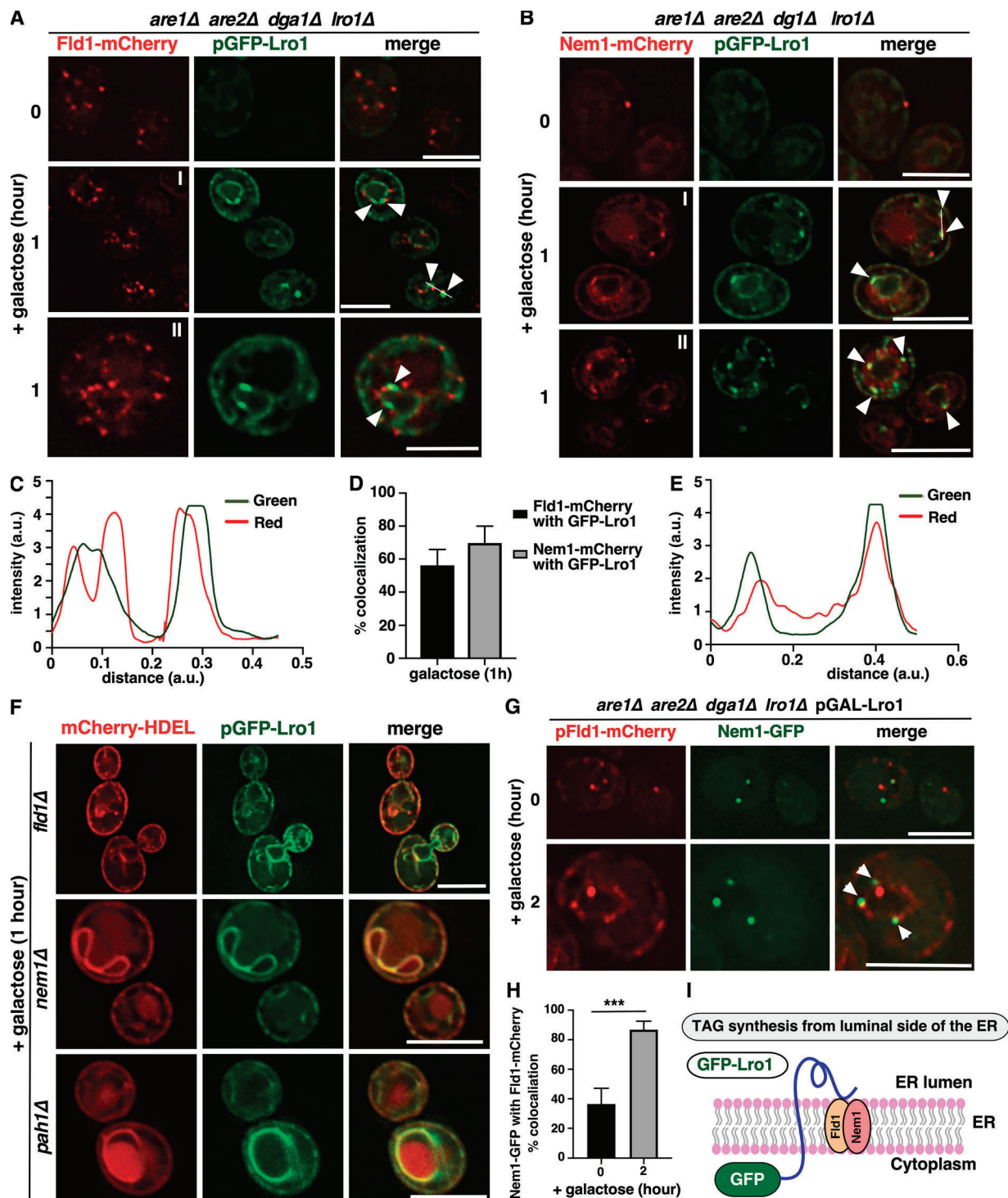
http://doc.rero.ch

5

Figure 3. ER sites marked by Fld1 and Nem1 recruit native Lro1. (A and B) ER subdomains marked by Fld1 and Nem1 recruit native Lro1. 4ΔKO cells expressing Fld1-mCherry (A) or Nem1-mCherry (B) and coexpressing native GFP-Lro1 from a galactose-inducible promoter. Cells show punctate distribution of Fld1-mCherry and Nem1-mCherry (0 h). Upon induction, GFP-Lro1 colocalizes with Fld1-mCherry and Nem1-mCherry (1 h). White arrowheads indicate co-localization of Lro1 with Fld1 (A) and Nem1 (B), respectively. Two examples of the 1 h time points are shown (I, II) for A and B. Scale bars, 5 μm. **(C and E)** Line trace of signal intensity along the white line shown in A (I) and B (I), respectively. **(D)** Quantification of colocalization between Fld1 or Nem1 foci with Lro1. Data are means ± SD, n > 50 cells; **, P < 0.005. **(F)** Cells missing Fld1, Nem1, or Pah1 fail to recruit GFP-Lro1 into discrete foci. Cells expressing native GFP-Lro1 and coexpressing mCherry-HDEL to mark the ER were cultured in galactose-containing media for 1 h. Scale bars, 5 μm. **(G and H)** Colocalization between Fld1 and Nem1 during LD biogenesis. 4ΔKO cells expressing genomic Nem1-GFP and coexpressing Fld1-mCherry under a constitutive *ADH1* promoter, together with Lro1. Colocalization between Nem1 and Fld1 denoted by white arrowheads (G) was quantified after galactose induction of Lro1 for 2 h (H). Data are means ± SD, n > 50 cells; ***, P < 0.0005. Scale bars, 5 μm. **(I)** Cartoon illustrating recruitment of native Lro1 at Fld1 and Nem1 sites.

4ΔKO cells expressing genomic Nem1-GFP, coexpressing Fld1-mCherry, and native Lro1 under galactose-inducible promoter were analyzed. By 2 h of GAL-Lro1 induction, ~85% of Nem1-GFP colocalized with Fld1-mCherry (Fig. 3, G and H). Together, this set of results suggests that colocalization between Fld1 and Nem1 increases upon induction of LD biogenesis and that these ER subdomains recruit native Lro1 to promote localized TAG production and droplet assembly (Fig. 3 I).

ER subdomains containing Fld1 and Nem1 are enriched in DAG
Since GFP-Lro1 and GFP-FFAT-sLro1 are recruited to ER sites marked by Fld1 and Nem1, we wondered whether these sites are also enriched in DAG, because previous work suggested that sites of LD biogenesis become enriched in this lipid when LD biogenesis is induced (Joshi et al., 2018). To probe the distribution of DAG, we used a previously characterized ER-DAG sensor (Choudhary et al., 2018). This sensor is comprised of tandem C1 domains from human PKD (C1a/b-PKD) fused to GFP, which in turn is fused to the transmembrane region of Ubc6, a tail-anchored ER protein (Choudhary et al., 2018). In WT cells, the ER-DAG sensor shows ER distribution with few punctae that often colocalized with Fld1-mCherry and Nem1-mCherry (Fig. S4 A). When cells were grown in the presence of oleic acid (OA) to stimulate the production of LDs, the DAG-sensor mostly localized to punctae containing Fld1 or Nem1 (Fig. 4 A). Under these conditions, the ER-DAG sensor showed ~91% colocalization with Fld1 and ~95% with Nem1 (Fig. 4 B). 4ΔKO cells also showed punctate DAG distribution similar to WT cells, and the ER-DAG sensor colocalized with Fld1 and Nem1 sites even in the absence of LDs (Fig. S4 B). However, in cells lacking Nem1, Spo7, or Pah1, the ER-DAG sensor failed to mark punctate and instead displayed uniform ER localization, probably due to altered DAG distribution throughout the ER (Fig. S4 C), suggesting that Nem1, Spo7, and Pah1 are required to produce a local pool of DAG at these ER subdomains.

To examine whether GFP-FFAT-sLro1 and native Lro1 also colocalize with the ER-DAG sensor, we examined 4ΔKO cells expressing an mCherry-tagged ER-DAG sensor and coexpressing either GFP-FFAT-sLro1 or GFP-Lro1 from a galactose-inducible promoter. By 1.5 h of induction, GFP-FFAT-sLro1 became highly enriched in puncta that colocalized with ER-DAG sensor (Fig. 4 C). Similar results were obtained with GFP-Lro1, although it did not become as enriched in puncta as GFP-FFAT-sLro1 (Fig. 4 C). Taken together, these data suggest that the TAG-synthase sLro1 and native Lro1 localize to ER sites enriched in DAG.

Enzymatic activity of sLro1 is required for its localization to ER subdomains
Next, we wondered whether the catalytic activity of Lro1 is required for its localization to ER subdomains. Therefore, we expressed WT sLro1 and a catalytically dead mutant version of sLro1 (H618A) fused to MBP-Scarlet-FFAT (MBP-Scarlet-FFAT-sLro1/sLro1[H618A]) in 4ΔKO cells. When grown in glucose, cells expressing Scarlet-FFAT-sLro1 lacked any detectable LDs, as revealed by BODIPY staining (Fig. S4 D). Upon galactose induction, Scarlet-FFAT-sLro1 expression resulted in production

of TAG as revealed by radiolabeling cells with [3H]palmitic acid (Fig. 4 D). However, the catalytic mutant version of sLro1, Scarlet-FFAT-sLro1[H618A], failed to form any detectable levels of TAG (Fig. 4 D). This indicates that Scarlet-FFAT-sLro1 is enzymatically active and that the H618A mutant version is indeed inactive. When expressed in 4ΔKO cells, Scarlet-FFAT-sLro1 localized to punctae that stained positive for BODIPY (Fig. 4 E). The catalytically inactive mutant enzyme, however, failed to generate BODIPY positive punctae (Fig. 4 E). To gain mechanistic insight into sLro1 recruitment to ER subdomains, we purified polyhistidine-tagged sLro1 and sLro1[H618A] from *Escherichia coli* cells (Fig. S4 E) and performed in vitro DAG binding using microscale thermophoresis (MST). This analysis revealed that both WT sLro1 and catalytic dead sLro1[H618A] bind to short chain DAG (C8:0) with comparable dissociation constant (K_d) values (Fig. 4, F and G). Although both sLro1 and sLro1[H618A] bind DAG in vitro, only the catalytically active enzyme localized to Fld1-marked ER sites (Fig. 4 H). These data suggest that DAG binding alone is not sufficient for sLro1 localization to ER subdomains but that the catalytic activity of sLro1 is required for a stable targeting to these domains.

Fld1 and Nem1 are both required to recruit the TAG-synthase
Next, we asked whether the TAG-synthase would still be recruited to Fld1- and Nem1-containing ER subdomains when either Fld1 or Nem1 was missing. Therefore, LD formation was induced in seipin mutant cells expressing genomic Nem1-mCherry and coexpressing either native Lro1 (GFP-Lro1) or the sLro1 (GFP-FFAT-sLro1; Fig. 5, A and B). While Nem1 still localized to ER subdomains in the absence of Fld1, these Nem1 punctae failed to recruit Lro1/sLro1. These results indicate that Fld1 activity at Nem1 sites is required for recruitment of the TAG-synthase. Similarly, in *nem1Δ* cells, Fld1-mCherry still localized to ER subdomains, but these Fld1 punctae failed to recruit Lro1/sLro1 (Fig. 5, C and D). This set of results indicates that the activity of both proteins, Fld1 and Nem1, is required at sites of LD biogenesis for the recruitment of the TAG-synthase (Fig. 5, E and F).

Next, we compared rates of TAG synthesis in cells lacking Fld1 or Nem1 and expressing GFP-FFAT-sLro1. Lack of Fld1 did not impair the rate of TAG synthesis when cells were labeled with [3H]palmitic acid (Fig. S4 F). This is consistent with previous studies that found that *fld1Δ* cells had normal levels of neutral lipids (Wang et al., 2016). However, *nem1Δ* mutant cells showed a reduced rate of TAG formation, and this was rescued by expression of a hyperactive allele of Pah1 (Pah1-7P), which bypasses the requirement of Nem1 for activation of Pah1 (Fig. S4 F; O'Hara et al., 2006). This suggests that DAG formation in *nem1Δ* mutant cells might be limiting for recruitment of GFP-FFAT-sLro1. In support of this notion, *nem1Δ* cells expressing Pah1-7P showed normal recruitment of GFP-FFAT-sLro1 at Fld1 sites (Fig. 5 G).

ER subdomains defined by Fld1 and Nem1 recruit the LD biogenesis protein Yft2
If ER subdomains defined by Fld1 and Nem1 recruit the TAG-synthase to locally form LDs, one would expect that LD marker
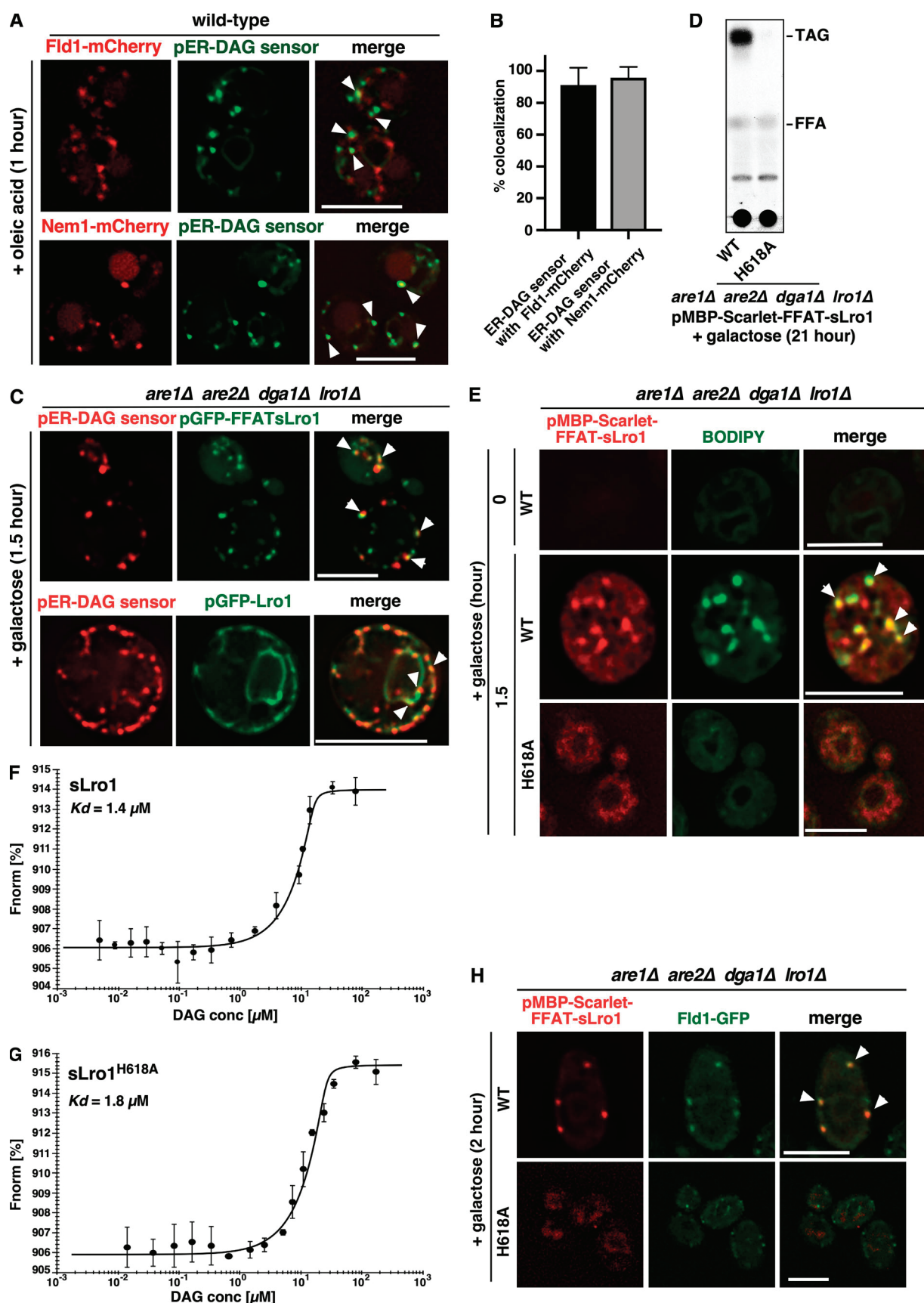
Figure 4. Enzymatic activity of TAG-synthase sLro1 is required for its recruitment to DAG-enriched ER subdomains. (A) Induction of LD formation by OA results in elevated DAG levels at Fld1 and Nem1 sites. WT cells expressing Fld1-mCherry or Nem1-mCherry and coexpressing the GFP-tagged ER-DAG

sensor were diluted and incubated in SC media containing 0.1% OA for 1 h. White arrowheads indicate colocalization of the ER-DAG sensor with Fld1 or Nem1 punctae. Scale bars, 5 µm. **(B)** Quantification of colocalization between ER-DAG sensor punctae with Fld1 and Nem1 1 h after OA addition. Data are means ± SD, *n* > 50 cells; ***, P < 0.0005. **(C)** Cytosolic sLro1 and native Lro1 colocalize with the DAG sensor. 4ΔKO cells expressing mCherry-tagged ER-DAG sensor and coexpressing GFP-FFAT-sLro1/GFP-Lro1 under galactose promoter. White arrowheads denote colocalization between the ER-DAG sensor and either sLro1 or Lro1. Scale bars, 5 µm. **(D)** Mutant sLro1 fails to produce TAG. 4ΔKO cells expressing WT sLro1 (Scarlet-FFAT-sLro1) or mutant sLro1 (Scarlet-FFAT-sLro1^{H618A}) were grown in galactose media containing [^{3}H]palmitic acid for 21 h. Lipids were extracted and separated by TLC. FFA, free fatty acid. **(E)** A catalytically inactive mutant of sLro1 fails to produce LDs. 4ΔKO cells expressing WT or mutant version of sLro1 from a galactose-inducible promoter were stained with BODIPY. White arrowheads denote colocalization between BODIPY-marked LDs and WT sLro1 punctae. Scale bars, 5 µm. **(F and G)** WT and mutant version of sLro1 bind DAG. In vitro binding of the short chain DAG (C8:0) by purified WT and mutant sLro1 was measured by MST. conc, concentration; Fnorm, normalized fluorescence. **(H)** Enzymatic activity of sLro1 is required for its colocalization with Fld1. 4ΔKO cells expressing WT or mutant version of sLro1 together with Fld1-GFP were switched to galactose media for 2 h. White arrowheads denote colocalization between WT sLro1 and Fld1. Scale bars, 5 µm.

proteins would also coenrich at these sites. Previously, we have reported that one of the yeast FIT2 proteins, Yft2, becomes enriched at sites of LD biogenesis (Choudhary et al., 2018). Yft2 together with Scs3 play an important role in LD biogenesis, as cells missing these ER proteins have defects in LD formation (Choudhary et al., 2015). We wondered whether Yft2 would colocalize with Fld1 and Nem1. Thus, we used an inducible strain lacking three of the neutral lipid–synthesizing proteins, having the fourth under a galactose-inducible promoter, *GAL-LRO1 are1Δ are2Δ dga1Δ* (hereafter 3ΔKO). This strain expressed Fld1-mCherry or Nem1-mCherry and coexpressed Yft2-sf-GFP, a superfolding variant of GFP (Pédelacq et al., 2006). In cells lacking LDs, Yft2 uniformly stained the ER (Fig. 6, A and B; 0-h time point). However, upon induction of TAG production, Yft2 concentrated into punctae that ~100% colocalized with Fld1 or Nem1 (Fig. 6, A–D; 1.5-h time point). Next, we determined whether other ER membrane proteins would show a similar enrichment at LD biogenesis sites. We visualized the localization of the ER membrane protein Sec63-GFP in 3ΔKO cells expressing Fld1-mCherry. When these cells were grown in galactose media to produce LDs, Sec63-GFP did not show any coenrichment with Fld1-mCherry–marked sites of LD biogenesis (Fig. S4 G), suggesting that proteins that are not involved in LD biogenesis do not enrich at Fld1 sites.

Yft2 requires Nem1, but not Fld1, at LD biogenesis sites
To determine whether lack of Fld1 from LD biogenesis sites would impair recruitment of Yft2, we generated *fld1Δ* 3ΔKO cells expressing Nem1-mCherry and Yft2-sf-GFP. Lack of Fld1 did not abrogate the recruitment of Yft2 at Nem1 sites upon induction of TAG synthesis (Fig. 6 E), suggesting that the yeast FIT2 protein, Yft2, does not require Fld1 to get recruited at LD biogenesis sites (Fig. 6 F). Previously, we have shown that Yft2 and Scs3 regulate DAG levels at sites of LD biogenesis in the ER (Choudhary et al., 2018). Since Nem1 regulates DAG production, we wondered whether Yft2 enrichment at LD biogenesis sites is dependent on Nem1. In *NEM1* WT cells expressing Fld1-mCherry and Yft2-sf-GFP, Yft2 showed uniform ER staining at the beginning of OA-stimulated induction of LD biogenesis. However, after 1.5 h, Yft2 colocalized with Fld1 (Fig. 6 G). When we performed similar OA supplementation experiments in *nem1Δ* cells, Yft2 did not enrich at discrete ER sites (Fig. 6 H). Although deletion of Nem1 did not affect the localization of Fld1, the recruitment of Yft2 to Fld1 subdomains depends on Nem1 (Fig. 6, H and I). In agreement with this, expression of Pah1-7P rescued the recruitment of Yft2

at Fld1 sites in *nem1Δ* cells (Fig. 6 J). These data indicate that DAG levels affect the colocalization of Yft2 and Fld1 and support the idea that both Fld1 and Nem1 are needed to establish ER subdomains for LD formation.

Lack of FIT2 does not abrogate the recruitment of the TAG-synthase
Next, we investigated whether FIT2 proteins Yft2 and Scs3 are necessary for the localization of GFP-FFAT-sLro1. Hence, we tagged Fld1-mCherry in *yft2Δ scs3Δ* double mutants expressing GFP-FFAT-sLro1. Lack of FIT2 proteins had no effect on the localization of Fld1, and these Fld1 subdomains were functional in recruiting GFP-FFAT-sLro1 (Fig. 7 A). Since Fld1 and Nem1 mark ER sites of LD biogenesis, and Yft2 requires Nem1 to get recruited at Fld1 sites (Fig. 6, G–J), we evaluated the distribution of DAG in *yft2Δ scs3Δ* double mutant cells. Therefore, we used WT and *yft2Δ scs3Δ* cells expressing Fld1-mCherry and coexpressing the ER-DAG sensor. Unlike WT cells, where the DAG probe shows uniform ER distribution with a few spots that colocalized with Fld1, *yft2Δ scs3Δ* mutant cells showed large blobs containing both the ER-DAG sensor and Fld1 (Fig. 7 B). These results indicate that FIT2 activity is required downstream of Fld1 and Nem1 for proper DAG distribution at sites of LD biogenesis (Fig. 7, B and C).

Pex30 is required downstream of Fld1, Nem1, and Yft2 to recruit the TAG-synthase
We wondered whether other proteins involved in LD biogenesis are important in organizing ER subdomains to facilitate droplet assembly. Pex30 is a reticulon-like, ER membrane–shaping protein (Joshi et al., 2016) that localizes to Fld1-containing ER subdomains (Joshi et al., 2018; Wang et al., 2018). In cells lacking Fld1, Pex30 mislocalizes to one large punctum per cell (Joshi et al., 2018; Wang et al., 2018). Since we find that Fld1 and Nem1 define ER sites of LD biogenesis, we wondered whether Pex30 plays a role upstream or downstream of Fld1 and Nem1 in organizing these ER subdomains. Hence, we tagged Fld1-mCherry and Nem1-mCherry in *pex30Δ* mutants expressing GFP-FFAT-sLro1. Unlike in *fld1Δ* cells, where Pex30 is completely mislocalized to one punctum per cell (Joshi et al., 2018; Wang et al., 2018), in cells missing Pex30, Fld1 or Nem1 still localized to discrete spots in the ER (Fig. 7, D and E). This suggests that localization of Fld1 and Nem1 proteins is independent of Pex30. However, in the absence of Pex30, these subdomains failed to recruit GFP-FFAT-sLro1 (Fig. 7, D and E). This indicates that Pex30 plays an indispensable role downstream of Fld1 and Nem1 in organizing ER subdomains for LD biogenesis (Fig. 7 G).
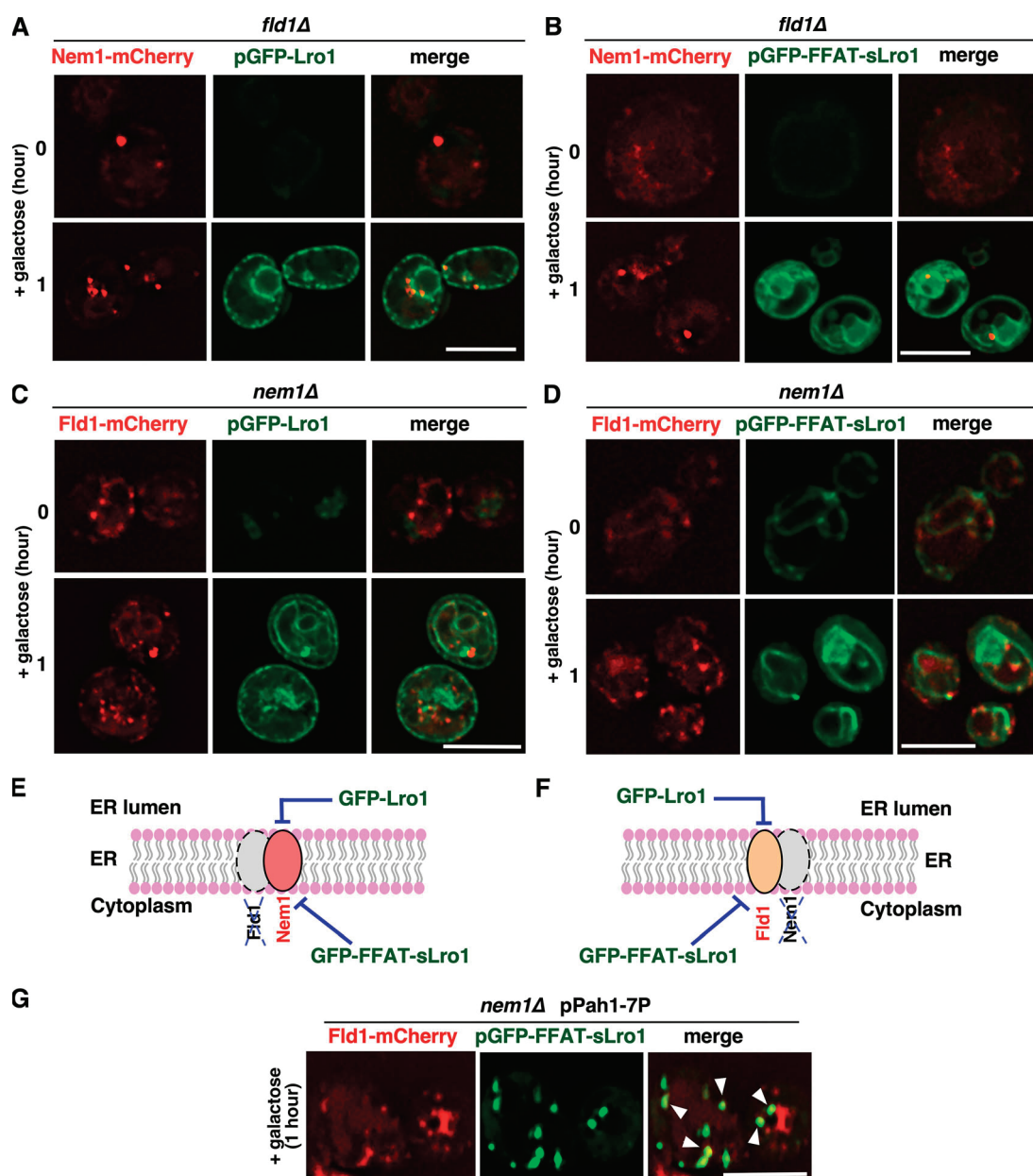
Figure 5. **Fld1 and Nem1 are both required for recruitment of the TAG-synthase. (A and B)** Fld1 is required to recruit both native and cytosolic Lro1 to Nem1 sites. *fld1Δ* cells expressing Nem1-mCherry and coexpressing native GFP-Lro1 (A) or cytosolic GFP-FFAT-sLro1 (B) from a galactose-inducible promoter. Scale bars, 5 μm. **(C and D)** Nem1 is required to recruit Lro1 to Fld1 sites. *nem1Δ* cells expressing Fld1-mCherry and coexpressing native GFP-Lro1 (C) or cytosolic GFP-FFAT-sLro1 (D) from a galactose-inducible promoter. Scale bars, 5 μm. **(E and F)** Fld1 and Nem1 together constitute functional ER sites for LD biogenesis. Cartoon depicting ER subdomains containing both Fld1 and Nem1 as a prerequisite for the recruitment of the native GFP-Lro1 or the cytosolic GFP-FFAT-sLro1. **(G)** Expression of Pah1-7P in *nem1Δ* cells rescues the defect in recruitment of the TAG-synthase. *nem1Δ* cells expressing Fld1-mCherry, and coexpressing both Pah1-7P, and GFP-FFAT-sLro1. White arrowheads denote colocalization between GFP-FFAT-sLro1 and Fld1-mCherry. Scale bar, 5 μm.

To determine whether Yft2 functions upstream or downstream of Pex30, we generated *pex30Δ* cells expressing Fld1-mCherry or Nem1-mCherry and coexpressing Yft2-sf-GFP. When these cells were grown in OA media to stimulate production of LDs, Yft2 showed punctate distribution and mostly colocalized with Fld1 or Nem1 (Fig. 7 F). This suggests that localization of Yft2 at Fld1 or Nem1 sites is independent of Pex30 and implies that Pex30 is required downstream of Fld1, Nem1, and Yft2 in organizing ER subdomains for

the recruitment of GFP-FFAT-sLro1 at LD biogenesis sites (Fig. 7 H).

Role of yeast PLIN proteins in organizing ER sites of LD biogenesis

Next, we tested whether Pet10, a yeast homologue of mammalian perilipins, is required for the recruitment of GFP-FFAT-sLro1 at Fld1 or Nem1 sites (Gao et al., 2017). Perilipins are scaffolding proteins that stabilize LDs and play an important role
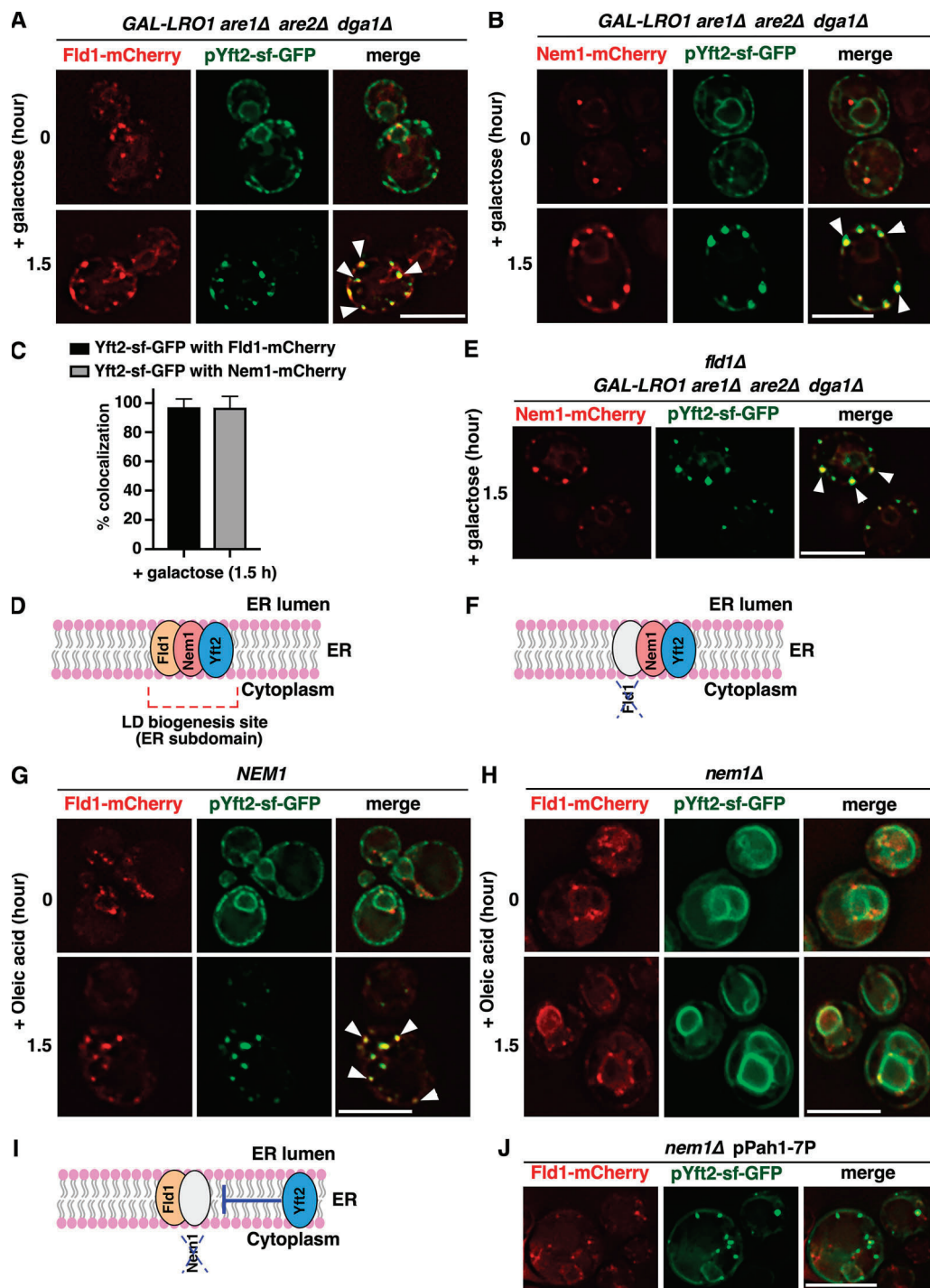
10

A *GAL-LRO1 are1Δ are2Δ dga1Δ*

Fld1-mCherry | pYft2-sf-GFP | merge

+ galactose (hour) 0

1.5

B *GAL-LRO1 are1Δ are2Δ dga1Δ*

Nem1-mCherry | pYft2-sf-GFP | merge

+ galactose (hour) 0

1.5

C
- Yft2-sf-GFP with Fld1-mCherry
- Yft2-sf-GFP with Nem1-mCherry

% colocalization

+ galactose (1.5 h)

E *fld1Δ GAL-LRO1 are1Δ are2Δ dga1Δ*

Nem1-mCherry | pYft2-sf-GFP | merge

+ galactose (hour) 1.5

D
ER lumen
Fld1 Nem1 Yft2
ER
Cytoplasm
LD biogenesis site
(ER subdomain)

F
ER lumen
Nem1 Yft2
ER
Cytoplasm
Fld1

G *NEM1*

Fld1-mCherry | pYft2-sf-GFP | merge

+ Oleic acid (hour) 0

1.5

H *nem1Δ*

Fld1-mCherry | pYft2-sf-GFP | merge

+ Oleic acid (hour) 0

1.5

I
ER lumen
Fld1 Yft2
ER
Cytoplasm
Nem1

J *nem1Δ pPah1-7P*

Fld1-mCherry | pYft2-sf-GFP | merge

Figure 6.   **ER subdomains marked by Fld1 and Nem1 recruit Yft2. (A and B)** Yft2 concentrates at Fld1- and Nem1-containing ER sites. 3ΔKO cells expressing Fld1-mCherry (A) or Nem1-mCherry (B) and coexpressing Yft2-sf-GFP were transferred to galactose media. White arrowheads indicate colocalization of Yft2 with Fld1 (A) or Nem1 (B). **(C)** Quantification of colocalization of Yft2 with Fld1 and Nem1. Data are means ± SD, *n* > 50 cells. **(D)** Cartoon depicting ER subdomain containing Fld1, Nem1, and Yft2. **(E)** Localization of Yft2 at Nem1 sites is independent of Fld1. *fld1Δ* 3ΔKO cells expressing Nem1-mCherry and coexpressing Yft2-sf-GFP were grown as described in A. White arrowheads indicate colocalization of Yft2 with Nem1. **(F)** Cartoon showing that the colocalization of Yft2 with Nem1 is independent of Fld1. **(G and H)** Yft2 requires Nem1 at sites of LD biogenesis. *NEM1* (G) and *nem1Δ* (H) cells expressing Fld1-mCherry and coexpressing Yft2-sf-GFP were grown in SC media, resuspended into fresh media containing 0.1% OA, and visualized after 1.5 h. White arrowheads denote colocalization of Yft2 with Fld1 foci in G. Scale bar, 5 μm. **(I)** Cartoon depicting colocalization between Yft2 and Fld1 is dependent on Nem1. **(J)** DAG levels affect the localization of Yft2 and Fld1. *nem1Δ* cells expressing Fld1-mCherry, Yft2-sf-GFP, and coexpressing Pah1-7P were grown to early stationary phase in SC media. White arrowheads denote colocalization of Yft2 with Fld1 foci. Scale bar, 5 μm.
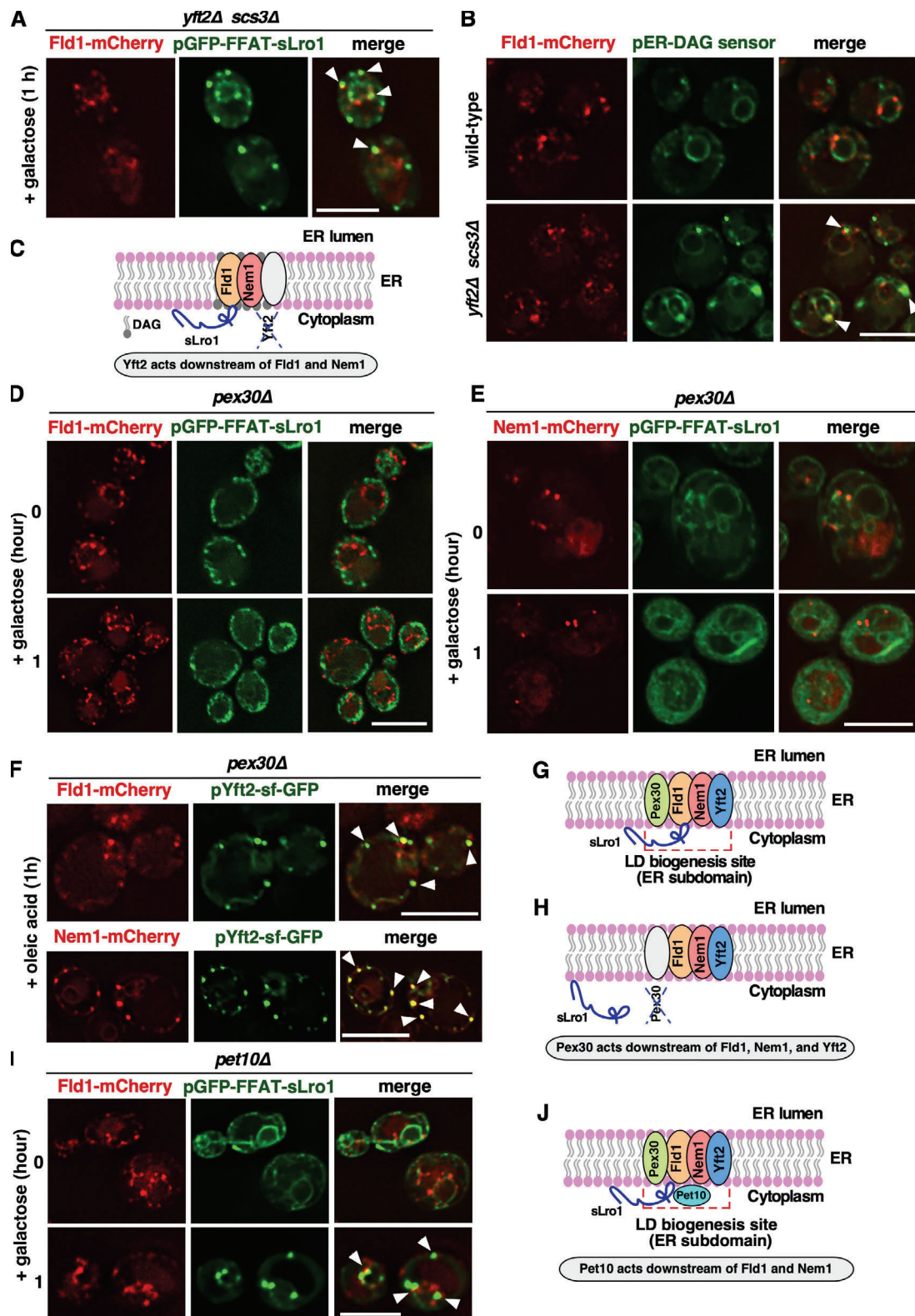
Figure 7. Epistatic relation of proteins at LD biogenesis sites. (A) Lack of FIT proteins does not abrogate recruitment of GFP-FFAT-sLro1 at Fld1 sites. *yft2Δ scs3Δ* double mutant cells expressing Fld1-mCherry and coexpressing GFP-FFAT-sLro1 were switched to galactose media for 1 h. White arrowheads indicate colocalization of Fld1 with sLro1. **(B)** Cells lacking FIT proteins have elevated DAG levels at Fld1 sites. WT and *yft2Δ scs3Δ* double mutant cells expressing Fld1-mCherry and coexpressing the GFP-tagged ER-DAG sensor were grown to early stationary phase. Arrowheads indicate colocalization of Fld1 foci with the DAG-sensor punctae. **(C)** Cartoon showing accumulation of DAG at Fld1- and Nem1-marked ER subdomains when these sites are missing Yft2. **(D and E)** Pex30 acts downstream of Fld1 and Nem1 in recruiting GFP-FFAT-sLro1 to sites of LD biogenesis. *pex30Δ* mutant cells expressing Fld1-mCherry (D) or Nem1-mCherry (E) and coexpressing GFP-FFAT-sLro1 were switched to galactose-containing media for the indicated time. **(F)** Yft2 functions independently of Pex30 at sites of LD

12

biogenesis. *pex30Δ* mutant cells expressing Fld1-mCherry or Nem1-mCherry and coexpressing Yft2-sf-GFP were diluted into fresh SC media containing 0.1% OA and imaged after 1 h. White arrowheads indicate colocalization of Yft2 with Fld1 or Nem1 punctae. **(G and H)** Cartoon illustrating the localization of Fld1, Nem1, Yft2, and Pex30 at ER subdomains to constitute functional LD biogenesis sites (G). Absence of Pex30 from these sites does not affect the localization of Fld1, Nem1, and Yft2, but these sites fail to recruit the sLro1 (H). **(I)** Lack of Pet10 does not impair the recruitment of GFP-FFAT-sLro1 at Fld1 sites. *pet10Δ* mutant cells expressing Fld1-mCherry and coexpressing GFP-FFAT-sLro1 were grown as described in D. Arrowheads denote colocalization of sLro1 with Fld1 foci. Scale bar, 5 μm. **(J)** Cartoon illustrating localization of sLro1 at Fld1 sites in the absence of Pet10.

in regulating storage and turnover of neutral lipids (Brasaemle, 2007). Yeast cells missing Pet10 display delayed LD biogenesis, decreased TAG accumulation in the ER, and fusogenic LDs (Gao et al., 2017). *pet10Δ* mutant cells expressing Fld1-mCherry or Nem1-mCherry and coexpressing GFP-FFAT-sLro1 showed no aberrant localization of Fld1 or Nem1 and did not impair the recruitment of GFP-FFAT-sLro1 at Fld1 sites (Fig. 7 I and Fig. S4 H). This suggests that Pet10 acts downstream of Fld1 and Nem1 and that the yeast perilipin homologue is not required for the recruitment of the TAG-synthase at Fld1 or Nem1 sites (Fig. 7 J).

Loss of seipin results in the formation of ectopic LDs

Our results suggest that Fld1 and Nem1 define ER subdomains for the recruitment of the TAG-synthase and the LD biogenesis factors Yft2 and Pex30. Thus, we tested whether the LD marker Erg6 would colocalize with Fld1 or Nem1 when cells are stimulated to produce LDs. Therefore, we generated 3ΔKO cells expressing genomic Fld1-mCherry or Nem1-mCherry and coexpressing Erg6-GFP from a plasmid. Prior to induction, Fld1 and Nem1 showed punctate localization in cells devoid of neutral lipids, and Erg6 was uniformly distributed over the ER membrane (Fig. 8, A and B). Upon galactose induction, Erg6-GFP rapidly colocalized to ∼100% with Fld1 or Nem1 spots (Fig. 8, A–C). Upon continued TAG synthesis, mature LDs remained associated with Fld1 or Nem1 sites (Fig. 8, A and B), in agreement with previous findings showing that Fld1 and Nem1 localize to ER–LD contact sites (Adeyo et al., 2011; Grippa et al., 2015; Wolinski et al., 2015).

The fact that *fld1Δ* does not impair the localization of Nem1 into discrete ER sites made us wonder whether Erg6 would still localize to Nem1 sites in the absence of Fld1. To examine this possibility, we used an inducible mutant lacking Fld1 (*fld1Δ* 3ΔKO) expressing Nem1-mCherry and Erg6-GFP. In cells lacking LDs, Erg6 showed uniform ER localization, whereas Nem1 showed punctate ER distribution (Fig. 8 D). Upon galactose induction, however, most of the cells failed to produce LDs as evidenced by few Erg6 spots (Fig. 8 D). Only ∼10% of cells showed a single Erg6 punctum per cell, which did not colocalize with Nem1 (Fig. 8, D–F). Deletion of Fld1 does not impair the rate of TAG synthesis; however, TAG accumulates throughout the ER membrane (Cartwright et al., 2015). In agreement with this, we find that in *fld1Δ* cells, induction of TAG synthesis resulted in accumulation of BODIPY throughout the ER, with a few BODIPY puncta that did not colocalize with Nem1 (Fig. S4 I). This suggests that Fld1 activity at Nem1 sites plays a crucial role in the biogenesis of LDs, as in the absence of Fld1, TAG synthesis occurred throughout the ER. Fld1 is required for the proper localization of Pex30 (Joshi et al., 2018; Wang et al., 2018),

although lack of Fld1 has no effect on the localization of Nem1 and Yft2 (Fig. 6 E). Absence of Fld1 or Pex30 results in failure to recruit the TAG-synthase at ER subdomains containing Nem1 and Yft2, leading to ectopic TAG synthesis (Fig. 8 G). Overall, these results indicate that LD biogenesis proteins Fld1, Nem1, Yft2, Pex30, Pet10, Erg6, and Lro1 cooperate to define ER subdomains that are likely enriched in certain lipids to facilitate localized TAG synthesis and droplet formation (Fig. 8 H).

Induction of TAG-synthase Dga1 results in LD formation at Fld1 and Nem1 sites

Next, we asked whether induction of the second TAG-synthase in yeast, Dga1, would also result in LD formation at Fld1 and Nem1 ER sites. Dga1 has a hairpin topology, having both N and C termini exposed toward the cytosol, and catalyzes TAG formation from the cytosolic leaflet of the ER using membrane-embedded DAG and cytosolic acyl-CoA as substrates (Oelkers et al., 2002; Sorger and Daum, 2002). Therefore, we generated 4ΔKO cells expressing Fld1-mCherry (Fig. S5, A and C) or Nem1-mCherry (Fig. S5, B and D) and coexpressing Dga1 from a galactose-inducible promoter. Upon induction, BODIPY-marked LDs rapidly appeared at Fld1 and Nem1 sites (Fig. S5, A and B), and these sites were also marked by Erg6-GFP (Fig. S5, C and D). Next, we investigated whether the TAG-synthase Dga1 also became enriched at Fld1 and Nem1 sites. Therefore, 4ΔKO cells expressing Fld1-GFP (Fig. S5 E) or Nem1-GFP (Fig. S5 F) together with Dga1-mCherry from a galactose promoter were analyzed. Prior to induction, Fld1 and Nem1 showed punctate localization (Fig. S5, E and F). Upon galactose induction, these punctae rapidly became stained by Dga1-mCherry (Fig. S5, E and F). These data suggest that not only Lro1 but also Dga1 localizes to Fld1- and Nem1-marked ER subdomains during induction of LD biogenesis to promote localized TAG production and droplet assembly (Fig. S5 G).

Discussion

What determines the sites of LD biogenesis in the ER is not well understood. In this study, we demonstrate that biogenesis of LDs occurs at predefined discrete ER subdomains marked by Fld1 and Nem1. The localization of both Fld1 and Nem1 at these specialized ER sites is independent of neutral lipid synthesis or the presence of LDs. Fld1 and Nem1 localize independent of each other, but both are required to create functional sites of LD biogenesis. These Fld1- and Nem1-marked ER sites become enriched with LD biogenesis proteins, including Yft2, Pex30, Pet10, Erg6, and Lro1. Based on these data, we propose a model for the stepwise assembly of factors for initiating LD biogenesis (Fig. 9).

In cells devoid of neutral lipids, Fld1 and Nem1 localize to discrete ER sites (Fig. 9, steps a and b). We do not yet know the
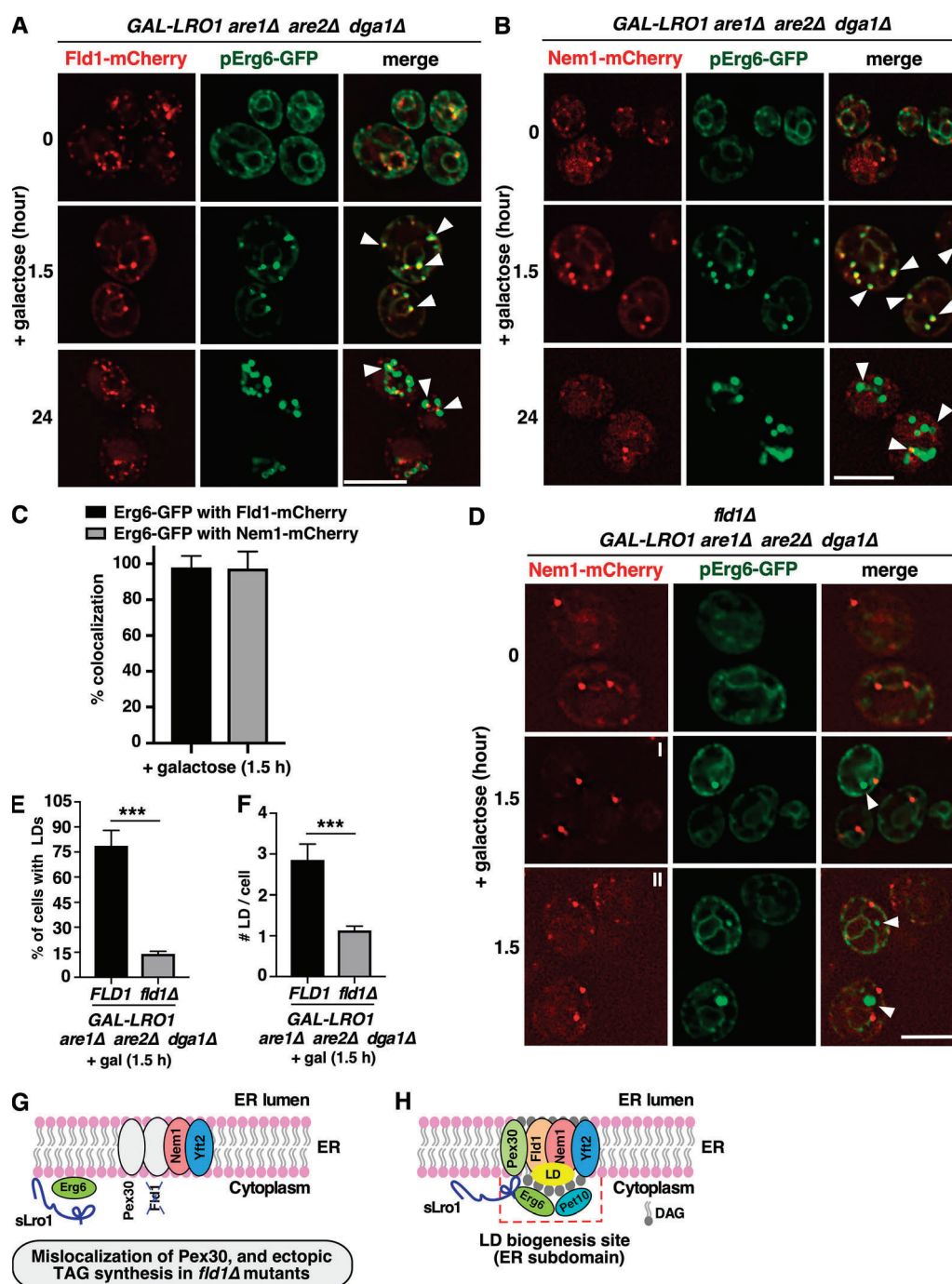
Figure 8. Absence of Fld1 from LD biogenesis sites results in ectopic droplet formation. (A and B) LDs form at Fld1- and Nem1-marked ER sites. 3ΔKO expressing Fld1-mCherry (A) or Nem1-mCherry (B) and coexpressing Erg6-GFP were transferred to galactose-containing media for the indicated time. White arrowheads denote colocalization between Erg6 with Fld1 (A) or Nem1 (B). **(C)** Quantification of colocalization of Erg6 with Fld1 and Nem1. Data are means ± SD, *n* > 50 cells. **(D)** LDs fail to form at Nem1 sites in cells lacking Fld1. *fld1Δ* mutant cells (*fld1Δ* 3ΔKO) expressing Nem1-mCherry and coexpressing Erg6-GFP were grown as described in A. White arrowheads indicate Erg6 punctae that do not colocalize with Nem1. Scale bar, 5 μm. **(E and F)** Quantification of cells with at least 1 LD (E), or number of LDs per cell (F) for images shown in D. Data are means ± SD, *n* > 50 cells; ***, P < 0.0005. **(G)** Cartoon depicting lack of Fld1 from LD biogenesis sites does not affect the localization of Nem1 and Yft2 but results in mislocalization of Pex30 and failure to recruit the TAG-synthase. **(H)** Cartoon showing that ER subdomains containing Fld1, Nem1, Yft2, and Pex30 define sites for the localization of the TAG-synthase and droplet formation. Erg6 and Pet10 bind to newly formed LDs from the cytosolic side.

determinant for this punctate localization. It is possible that specific proteins, lipids, or possibly a combination of both facilitate the recruitment of Fld1 and Nem1 into discrete spots in the ER in cells lacking LDs. This should be investigated in further studies. Almost all of the Nem1 punctae appear to be stable and immobilized in the ER, whereas some of the Fld1 punctae move along the ER, while others are stable. It is likely that only the sites at which both Fld1 and Nem1 colocalize (Fld1/Nem1 sites)
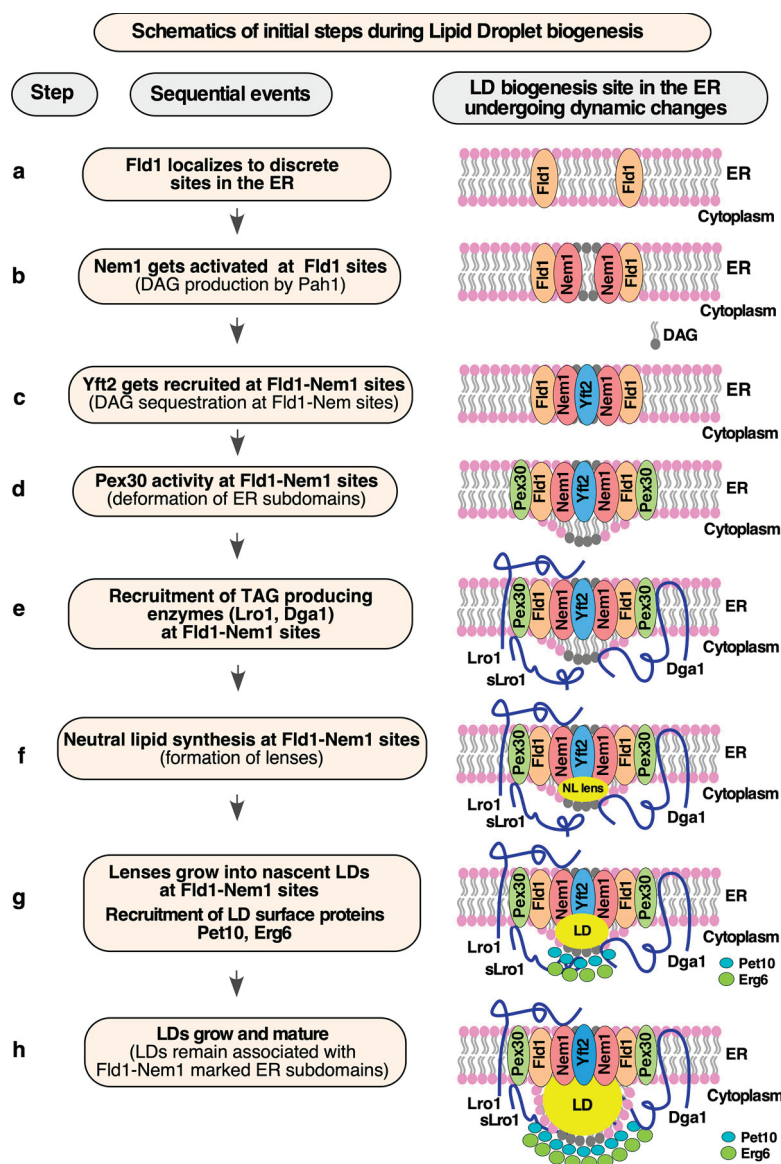
14

Schematics of initial steps during Lipid Droplet biogenesis

Step	Sequential events	LD biogenesis site in the ER undergoing dynamic changes
a	Fld1 localizes to discrete sites in the ER	
b	Nem1 gets activated at Fld1 sites (DAG production by Pah1)	
c	Yft2 gets recruited at Fld1-Nem1 sites (DAG sequestration at Fld1-Nem sites)	
d	Pex30 activity at Fld1-Nem1 sites (deformation of ER subdomains)	
e	Recruitment of TAG producing enzymes (Lro1, Dga1) at Fld1-Nem1 sites	
f	Neutral lipid synthesis at Fld1-Nem1 sites (formation of lenses)	
g	Lenses grow into nascent LDs at Fld1-Nem1 sites. Recruitment of LD surface proteins Pet10, Erg6	
h	LDs grow and mature (LDs remain associated with Fld1-Nem1 marked ER subdomains)	

Figure 9. **Model of LD formation at discrete ER subdomains defined by Fld1 and Nem1.** Cartoon showing the order of events (steps a to h) occurring at predefined ER subdomains for efficient LD formation. Fld1- and Nem1-marked ER subdomains undergo sequential enrichment with LD biogenesis factors, thereby promoting localized TAG production and droplet assembly.

become functional for droplet assembly. Consistent with this, a new study identified seipin in complex with LD assembly factor 1 that copurified with TAG and defined sites of LD biogenesis (Chung et al., 2019). Moreover, mislocalization of seipin within the ER network to the nuclear envelop results in formation of LDs at these ectopic sites (Salo et al., 2019).

Fld1/Nem1 sites require the activity of Yft2, and Pex30, to ensure proper recruitment of the TAG-synthase, indicating that all four proteins (Fld1/Nem1/Yft2/Pex30) might work together in establishing ER subdomains permissive for localized TAG synthesis. Yft2 gets recruited to Fld1/Nem1 sites (Fig. 9, step c), possibly through direct binding of DAG and/or TAG (Gross et al., 2011). We have recently shown that Yft2 colocalizes with Fld1, Nem1, and the ER-DAG sensor (Choudhary et al., 2018). Pex30 acts downstream of Fld1, Nem1, and Yft2 to localize to LD biogenesis sites (Fig. 9, step d). The membrane-shaping property of Pex30 at these sites may facilitate the deformation of the ER bilayer to accommodate DAG and/or TAG. Indeed, Pex30 at LD

biogenesis sites colocalizes with Fld1, Nem1, and the ER-DAG sensor (Joshi et al., 2018; Wang et al., 2018).

Next, the TAG-synthase Lro1/Dga1 localizes to Fld1/Nem1/Yft2/Pex30 sites, resulting in the conversion of DAG to TAG and hence formation of lenses that grow into nascent LDs (Fig. 9, steps e–g). The fact that sLro1 goes to discrete ER sites suggests that its localization is driven by lipids since in the native Lro1 this portion of sLro1 is in the ER lumen and thus would not be available to specific protein–protein interactions in the cytosolic leaflet of the ER membrane. This hypothesis is supported by three findings: (1) native Lro1 and sLro1 colocalize with the ER-DAG sensor (Fig. 4 C), (2) purified sLro1 binds to DAG in vitro (Fig. 4 F), and (3) the mislocalization of Lro1 in *nem1Δ* cells is rescued by the expression of Pah1-7P (Fig. 5 G). In addition, proper recruitment of Lro1 requires the enzymatic activity of Lro1 as a catalytic dead point mutant of sLro1 (H618A) that still binds DAG in vitro fails to enrich at Fld1 sites in vivo (Fig. 4, G and H).

Nascent LDs are then recognized by cytosolic proteins such as the perilipin homologue Pet10 and Erg6, and the LD monolayer surface becomes stabilized, facilitating LD growth toward the cytosol (Fig. 9, steps g and h). Consistent with this proposition, artificial LDs embedded into giant unilamellar vesicles emerge toward the side having greater coverage with proteins and phospholipids, which reduces surface tension of the monolayer (Chorlay et al., 2019). Continued synthesis of TAG at Fld1/Nem1 sites results in maturation of LDs, which remain associated with the ER membrane at Fld1/Nem1 sites (Fig. 9, step h). In conclusion, our findings support the hypothesis that biogenesis of LDs is a well-orchestrated process that occurs at Fld1/Nem1/ Yft2/Pex30-marked discrete ER subdomains.

Materials and methods

Yeast strains and plasmids

Yeast strains and plasmids used in this study are listed in Table S1. Double- and triple-deletion mutants were generated either by mating or by PCR-based targeted homologous recombination to replace the ORF of the gene of interest with a deletion cassette followed by a marker rescue strategy (Gueldener et al., 2002). Chromosomally C-terminal–tagged versions of reporter proteins (Erg6-mCherry, Nem1-mCherry, Fld1-mCherry, Fld1-GFP, Nem1-GFP) were constructed using PCR-based homologous recombination (Longtine et al., 1998). The cassette yEmCherry-HIS5MX6 was obtained from J. Nunnari (University of California, Davis, Davis, CA). To construct the plasmid pGAL1-GFP-Lro1 (aa 1–661), or pGAL1-GFP-sLro1(aa 98–661), corresponding regions of LRO1 were amplified by PCR from S. cerevisiae genomic DNA and inserted into the plasmid pRS426, thereby expressing GFP fused to the N terminus of Lro1, or sLro1 under the GAL1 promoter. For plasmid pGAL1-GFP-FFAT, GFP was fused to a FFAT motif and inserted into pRS426 under GAL1 promoter. To create the plasmid pGAL1-MBP-GFP-FFAT-sLro1, the sLro1(aa 98–661) sequence was fused to FFAT, GFP, and the purification tag MBP and inserted into pRS426. To construct pGAL1-MBP-Scarlet-FFAT-sLro1, the sequence encoding Scarlet tag was amplified from laboratory plasmid collection and fused with FFAT, sLro1(aa 98–661), and MBP tag and inserted into pRS426. PCR-mediated site-directed mutagenesis was performed to generate sLro1[H618A] and cloned as a fusion with MBP-Scarlet-FFAT-sLro1[H618A] under GAL1 promoter into pRS426 vector. To generate pGAL1-ssKar2-GFP-sLro1, the sequence corresponding to sLro1(aa 98–661) was fused to GFP and the signal sequence of Kar2 (aa 1–42) and cloned into pRS426. For plasmid pGAL-Sec63(1–250)-GFP-sLro1, the sequence corresponding to 1–250 aa encoding TMDs 1–3 was fused with GFP and sLro1(aa 98–661) and inserted into pRS426 vector. We used plasmids expressing either mCherry-HDEL, RFP-HDEL, or GFP fused to Sec63 to label the ER. pADH-Fld1-mCherry was generated by amplifying the FLD1 gene from S. cerevisiae genomic DNA and inserting it into pRS415. The plasmids encoding Yft2-sf-GFP and the ER-DAG sensor (pADH-ER-DAG sensor) have been described previously (Choudhary et al., 2015, 2018). Plasmid expressing Pah1-7P was obtained from S. Siniossoglou (University of Cambridge, Cambridge, UK). All constructs were verified by sequencing.

Media and growth conditions

Cells were grown at 30°C in YPD medium (1% Bacto yeast extract, 2% Bacto Peptone, and 2% glucose) unless otherwise indicated. Cells containing plasmids were grown in synthetic complete (SC) media containing 6.7 g/liter yeast nitrogen base (United States Biologicals), an aa mix (United States Biologicals), and containing either 2% glucose, galactose, or raffinose. To grow cells in presence of fatty acids for induction of LD formation, SC media were supplemented with 0.1% OA (Sigma-Aldrich) in the presence of 1% Brij-58 (Sigma-Aldrich).

Fluorescence microscopy

For Fig. 1, E and F, and Fig. S1, B and C, cells were visualized and imaged live in culture media using an Olympus BX61 microscope, a UPlanApox100/1.35 lens, and a QImaging Retiga EX camera and processed using iVision software (version 4.0.5). Images being directly compared were obtained using identical microscope settings. For Figs. 2, 3, 4, 5, 6, 7, 8, S1 F, S2, S3, S4, and S5, live cell imaging was performed using a DeltaVision Elite imaging system (GE Healthcare). The DeltaVision Elite system is comprised of a wide-field inverted epifluorescence microscope (1X71; Olympus), equipped with a charge-coupled device camera (CoolSNAP HQ^2; Photometrics). Images were acquired using a U PLAN S-APO 100×1.42 NA oil immersion objective (Olympus) and a GFP or mCherry filter set. Stacks of seven images with a step size of 0.5 μm were deconvolved for 10 iterations using the conserved ratio method in softWoRx (Applied Precision). Single plane images are displayed. Time-lapse images were acquired every 1 s for 15 s with an exposure of 500 ms for Fig. S3 B and every 1 s for 60 s with an exposure of 500 ms for Fig. S3 C. Brightness and contrast were adjusted using Photoshop CC 2020 (Adobe Systems). Colocalization between GFP- and mCherry-marked punctae in acquired images was scored manually. Values were recorded in Excel (Microsoft) and analyzed in Prism 8.0 (GraphPad Software).

BODIPY staining to visualize LDs in yeast

To visualize LDs in yeast, cells expressing Erg6-mCherry were grown in YPD to early stationary phase and stained with 0.5 μg/ml BODIPY 493/503 (Invitrogen) for 5 min at RT. After washing once with 1× PBS, cells were visualized live using the GFP or mCherry filter set of the DeltaVision Elite (GE Healthcare).

Labeling with [³H]palmitic acid and quantification of lipids

To quantify neutral lipids and phospholipids, cells were grown in SC raffinose media overnight. Next-day cells were diluted to 1 OD$_{600}$ per ml and grown in SC galactose media containing 10 μCi/ml [³H]palmitic acid (10 mCi/ml; American Radiolabled Chemicals, Inc.). Cells were incubated with shaking at 30°C. 10 OD$_{600}$ units of cells were harvested at 10, 30, 60, 90, and 120 min (Fig. S4 F), at 10 min, 2 h, 4 h, and 21 h (Fig. 1 C), and at 21 h (Figs. 1 D, 4 D, and S1 G). Cells were lysed using a Precellys 24 homogenizer, lipids were extracted as described previously (Jacquier et al., 2011), and equal aliquots were brought to dryness. To quantify TAG and SEs, lipids were spotted onto silica gel 60 TLC plates (Merck) and developed with petroleum ether:diethylether:acetic acid (70:30:2, per vol). Glycerophospholipids

were separated by TLC as described previously (Vaden et al., 2005). TLC plates were exposed to a tritium-sensitive screen, visualized, and quantified using a phosphorimager (GE Healthcare). Brightness and contrast of the TIFF images were adjusted using ImageJ (National Institutes of Health).

Western blot analysis

Cells were grown overnight in SC raffinose media, diluted to 1 OD_{600} ml in SC galactose media, and cells corresponding to 3 OD_{600} units were harvested at 0-, 2-, 4-, 6-, and 21-h time points. Samples were extracted by NaOH, and proteins were precipitated using TCA and resuspended into sample buffer (Horvath and Riezman, 1994). Proteins were separated using SDS-PAGE and detected using a monoclonal antibody against GFP (mouse, 1:2,000 dilution, no. 11814460001; Roche Diagnostics) or Kar2 (rabbit, 1:5,000 dilution; Randy Schekman, University of California, Berkeley, Berkeley, CA) and using goat anti–rabbit IgG (H+L)-HRP conjugate (1:10,000 dilution, no. 1706515; Bio-Rad) and goat anti–mouse IgG (H+L)-HRP conjugates (1:10,000 dilution, no. 1706516; Bio-Rad). Subsequent detection occurred via peroxidase-coupled secondary antibodies and ECL Prime chemiluminescence substrate (Sigma-Aldrich) using an Image-Quant LAS 1000 biomolecular imager (GE Healthcare) and ImageQuant software. Western blot experiments were performed at least twice with similar results.

Quantification and statistical analysis

Unless otherwise stated, data were obtained from at least three independent experiments. The images presented are representative of the results obtained. Quantitative results are expressed as mean ± SD. Statistical analysis was performed with unpaired, two-tailed Student's t tests using Prism 8. P values < 0.05 are considered significant.

CLEM

For CLEM investigations, yeast cells were concentrated to a paste by vacuum filtration and subsequently cryoimmobilized with an HPM010 high pressure freezing machine (Bal-Tec). Automated freeze substitution in 0.1% uranyl acetate in acetone over a 72-h period and embedding in Lowicryl HM20 resin were performed using an EM AFS2 automatic freeze-substitution system (Leica Microsystems) as described previously (Kukulski et al., 2011; Thaller et al., 2019). Blocks were polymerized under UV light and cut in 300-nm-thick sections using an ultramicrotome (EM UC7; Leica Microsystems). Sections were picked up on carbon-coated 200 mesh grids (S160; Plano). 100- or 50-nm TetraSpeck fluorescent microspheres (Life Technologies) were adsorbed to the grid for the subsequent fiducial-based correlation between light and EM images. The fluorescence microscopy imaging of the sections was performed as detailed previously (Curwin et al., 2016; Kukulski et al., 2011) using a wide-field fluorescence microscope (IX81; Olympus) equipped with a PlanApo 60× 1.40 NA oil immersion objective (Olympus). In addition to the specific channel of the fluorescent protein(s) of interest, another channel was acquired to distinguish the specific signal from the TetraSpecks. Grids were then poststained for 5 min with 1% uranyl acetate and 3 min with Reynold's lead citrate. Tilt series were acquired with an FEI Tecnai F30 electron microscope run at 300 kV and controlled by a SerialEM (Mastronarde, 2005). Fluorescence microscopy maps were loaded using a point-based registration to low-magnification tiled acquisitions (2,300×) of the corresponding grid squares. High-magnification tilt series (15,500×) were then acquired at the selected fluorescent spot locations, using a SerialEM script (Schorb et al., 2019). Tomograms were then reconstructed using the IMOD software package (Kremer et al., 1996). For samples with 50-nm TetraSpeck beads, an intermediate acquisition at 4,700× was necessary to perform the alignment, as the beads were not visible in the lowest magnification. CLEM overlays were performed with a fiducial-based correlation using the plugin eC-CLEM in Icy (Paul-Gilloteaux et al., 2017) as described previously (Curwin et al., 2016). Tomograms were manually segmented using IMOD (Kremer et al., 1996).

Expression and purification of WT and mutant versions of sLro1

DNA encoding WT and mutant versions of sLro1 were cloned into the BamHI and XhoI sites of pET22b vector (Novagen, Merck), which contains a PelB signal sequence to direct the secretion of the expressed protein into the periplasmic space. Plasmids were transformed into *E. coli* BL21, and the proteins were expressed with a C-terminal polyhistidine tag after overnight lactose induction and growth of bacteria at 24°C. Cells were collected, lysed, and incubated with Ni-nitrilotriacetic acid (NTA) beads (Qiagen) per the manufacturer's instructions. The beads were washed and loaded onto a Ni^{2+}-NTA column (Qiagen), and the proteins were eluted in 60 mM NaH_2PO_4, 60 mM NaCl, and 300 mM imidazole, pH 8.0. The eluted proteins were applied to Zeba spin desalting columns (Thermo Fisher Scientific), and the buffer was exchanged to 60 mM NaH_2PO_4 and 10 mM NaCl, pH 8.0. Protein concentration was determined by Lowry assay using Folin reagent and BSA standard.

MST

MST experiments were performed using a Monolith NT.115 system (Nanotemper Technologies) to assess the binding of sLro1 and sLro1-H618A to short chain DAG (C8:0 DAG, no. 800800; Avanti Polar Lipids). Proteins were labeled using the RED-tris-NTA His tag protein-labeling kit (Nanotemper Technologies). Labeled protein was added to a serial dilution of unlabeled DAG, prepared in binding buffer (20 mM Tris, pH 7.5, 30 mM NaCl, and 0.05% Triton X-100). Samples were loaded into MST standard capillaries, and MST measurements were performed using 80% power setting. The K_d value was obtained by plotting the normalized fluorescence Fnorm against the logarithm of DAG concentrations. Experiments were performed in triplicates, and data were fitted using the K_d model with the MO.Affinity Analysis software.

Data availability

The data supporting the findings of this study are contained with the paper and its supplemental files.

Online supplemental material

Acknowledgments

References

Adeyo, O., P.J. Horn, S. Lee, D.D. Binns, A. Chandrahas, K.D. Chapman, and J.M. Goodman. 2011. The yeast lipin orthologue Pah1p is important for biogenesis of lipid droplets. *J. Cell Biol.* 192:1043–1055. https://doi.org/10.1083/jcb.201010111

Barbosa, A.D., H. Sembongi, W.M. Su, S. Abreu, F. Reggiori, G.M. Carman, and S. Siniossoglou. 2015. Lipid partitioning at the nuclear envelope controls membrane biogenesis. *Mol. Biol. Cell.* 26:3641–3657. https://doi.org/10.1091/mbc.E15-03-0173

Brasaemle, D.L.. 2007. Thematic review series: adipocyte biology. The perilipin family of structural lipid droplet proteins: stabilization of lipid droplets and control of lipolysis. *J. Lipid Res.* 48:2547–2559. https://doi.org/10.1194/jlr.R700014-JLR200

Cartwright, B.R., D.D. Binns, C.L. Hilton, S. Han, Q. Gao, and J.M. Goodman. 2015. Seipin performs dissectible functions in promoting lipid droplet

biogenesis and regulating droplet morphology. *Mol. Biol. Cell.* 26: 726–739. https://doi.org/10.1091/mbc.E14-08-1303

Chorlay, A., L. Monticelli, J. Verissimo Ferreira, K. Ben M'barek, D. Ajjaji, S. Wang, E. Johnson, R. Beck, M. Omrane, M. Beller, et al. 2019. Membrane Asymmetry Imposes Directionality on Lipid Droplet Emergence from the ER. *Dev. Cell.* 50:25–42. https://doi.org/10.1016/j.devcel.2019.05.003

Choudhary, V., N. Jacquier, and R. Schneiter. 2011. The topology of the triacylglycerol synthesizing enzyme Lro1 indicates that neutral lipids can be produced within the luminal compartment of the endoplasmatic reticulum: Implications for the biogenesis of lipid droplets. *Commun. Integr. Biol.* 4:781–784. https://doi.org/10.4161/cib.17830

Choudhary, V., N. Ojha, A. Golden, and W.A. Prinz. 2015. A conserved family of proteins facilitates nascent lipid droplet budding from the ER. *J. Cell Biol.* 211:261–271. https://doi.org/10.1083/jcb.201505067

Choudhary, V., G. Golani, A.S. Joshi, S. Cottier, R. Schneiter, W.A. Prinz, and M.M. Kozlov. 2018. Architecture of Lipid Droplets in Endoplasmic Reticulum Is Determined by Phospholipid Intrinsic Curvature. *Curr. Biol.* 28:915–926. https://doi.org/10.1016/j.cub.2018.02.020

Chung, J., X. Wu, T.J. Lambert, Z.W. Lai, T.C. Walther, and R.V. Farese, Jr.. 2019. LDAF1 and Seipin Form a Lipid Droplet Assembly Complex. *Dev. Cell.* 51:551–563. https://doi.org/10.1016/j.devcel.2019.10.006

Curwin, A.J., N. Brouwers, M. Alonso Y Adell, D. Teis, G. Turacchio, S. Parashuraman, P. Ronchi, and V. Malhotra. 2016. ESCRT-III drives the final stages of CUPS maturation for unconventional protein secretion. *eLife.* 5. e16299. https://doi.org/10.7554/eLife.16299

Fei, W., G. Shui, B. Gaeta, X. Du, L. Kuerschner, P. Li, A.J. Brown, M.R. Wenk, R.G. Parton, and H. Yang. 2008. Fld1p, a functional homologue of human seipin, regulates the size of lipid droplets in yeast. *J. Cell Biol.* 180: 473–482. https://doi.org/10.1083/jcb.200711136

Gao, Q., D.D. Binns, L.N. Kinch, N.V. Grishin, N. Ortiz, X. Chen, and J.M. Goodman. 2017. Pet10p is a yeast perilipin that stabilizes lipid droplets and promotes their assembly. *J. Cell Biol.* 216:3199–3217. https://doi.org/10.1083/jcb.201610013

Goh, V.J., J.S. Tan, B.C. Tan, C. Seow, W.Y. Ong, Y.C. Lim, L. Sun, S. Ghosh, and D.L. Silver. 2015. Postnatal Deletion of Fat Storage-inducing Transmembrane Protein 2 (FIT2/FITM2) Causes Lethal Enteropathy. *J. Biol. Chem.* 290:25686–25699. https://doi.org/10.1074/jbc.M115.676700

Grippa, A., L. Buxó, G. Mora, C. Funaya, F.Z. Idrissi, F. Mancuso, R. Gomez, J. Muntanyà, E. Sabidó, and P. Carvalho. 2015. The seipin complex Fld1/Ldb16 stabilizes ER-lipid droplet contact sites. *J. Cell Biol.* 211:829–844. https://doi.org/10.1083/jcb.201502070

Gross, D.A., C. Zhan, and D.L. Silver. 2011. Direct binding of triglyceride to fat storage-inducing transmembrane proteins 1 and 2 is important for lipid droplet formation. *Proc. Natl. Acad. Sci. USA.* 108:19581–19586. https://doi.org/10.1073/pnas.1110817108

Gueldener, U., J. Heinisch, G.J. Koehler, D. Voss, and J.H. Hegemann. 2002. A second set of loxP marker cassettes for Cre-mediated multiple gene knockouts in budding yeast. *Nucleic Acids Res.* 30. e23. https://doi.org/10.1093/nar/30.6.e23

Horvath, A., and H. Riezman. 1994. Rapid protein extraction from *Saccharomyces cerevisiae*. *Yeast.* 10:1305–1310. https://doi.org/10.1002/yea.320101007

Jacquier, N., V. Choudhary, M. Mari, A. Toulmay, F. Reggiori, and R. Schneiter. 2011. Lipid droplets are functionally connected to the endoplasmic reticulum in Saccharomyces cerevisiae. *J. Cell Sci.* 124: 2424–2437. https://doi.org/10.1242/jcs.076836

Joshi, A.S., X. Huang, V. Choudhary, T.P. Levine, J. Hu, and W.A. Prinz. 2016. A family of membrane-shaping proteins at ER subdomains regulates pre-peroxisomal vesicle biogenesis. *J. Cell Biol.* 215:515–529. https://doi.org/10.1083/jcb.201602064

Joshi, A.S., B. Nebenfuehr, V. Choudhary, P. Satpute-Krishnan, T.P. Levine, A. Golden, and W.A. Prinz. 2018. Lipid droplet and peroxisome biogenesis occur at the same ER subdomains. *Nat. Commun.* 9:2940. https://doi.org/10.1038/s41467-018-05277-3

Kadereit, B., P. Kumar, W.J. Wang, D. Miranda, E.L. Snapp, N. Severina, I. Torregroza, T. Evans, and D.L. Silver. 2008. Evolutionarily conserved gene family important for fat storage. *Proc. Natl. Acad. Sci. USA.* 105: 94–99. https://doi.org/10.1073/pnas.0708579105

Karanasios, E., A.D. Barbosa, H. Sembongi, M. Mari, G.S. Han, F. Reggiori, G.M. Carman, and S. Siniossoglou. 2013. Regulation of lipid droplet and membrane biogenesis by the acidic tail of the phosphatidate phosphatase Pah1p. *Mol. Biol. Cell.* 24:2124–2133. https://doi.org/10.1091/mbc.e13-01-0021

Kassan, A., A. Herms, A. Fernández-Vidal, M. Bosch, N.L. Schieber, B.J. Reddy, A. Fajardo, M. Gelabert-Baldrich, F. Tebar, C. Enrich, et al. 2013.

Acyl-CoA synthetase 3 promotes lipid droplet biogenesis in ER micro-domains. *J. Cell Biol*. 203:985–1001. https://doi.org/10.1083/jcb.201305142

Kremer, J.R., D.N. Mastronarde, and J.R. McIntosh. 1996. Computer visualization of three-dimensional image data using IMOD. *J. Struct. Biol*. 116: 71–76. https://doi.org/10.1006/jsbi.1996.0013

Kukulski, W., M. Schorb, S. Welsch, A. Picco, M. Kaksonen, and J.A. Briggs. 2011. Correlated fluorescence and 3D electron microscopy with high sensitivity and spatial precision. *J. Cell Biol*. 192:111–119. https://doi.org/10.1083/jcb.201009037

Loewen, C.J., A. Roy, and T.P. Levine. 2003. A conserved ER targeting motif in three families of lipid binding proteins and in Opi1p binds VAP. *EMBO J*. 22:2025–2035. https://doi.org/10.1093/emboj/cdg201

Longtine, M.S., A. McKenzie, III, D.J. Demarini, N.G. Shah, A. Wach, A. Brachat, P. Philippsen, and J.R. Pringle. 1998. Additional modules for versatile and economical PCR-based gene deletion and modification in Saccharomyces cerevisiae. *Yeast*. 14:953–961. https://doi.org/10.1002/(SICI)1097-0061(199807)14:10<953::AID-YEA293>3.0.CO;2-U

Mastronarde, D.N.. 2005. Automated electron microscope tomography using robust prediction of specimen movements. *J. Struct. Biol*. 152:36–51. https://doi.org/10.1016/j.jsb.2005.07.007

O'Hara, L., G.S. Han, S. Peak-Chew, N. Grimsey, G.M. Carman, and S. Siniossoglou. 2006. Control of phospholipid synthesis by phosphorylation of the yeast lipin Pah1p/Smp2p Mg2+-dependent phosphatidate phosphatase. *J. Biol. Chem*. 281:34537–34548. https://doi.org/10.1074/jbc.M606654200

Oelkers, P., D. Cromley, M. Padamsee, J.T. Billheimer, and S.L. Sturley. 2002. The DGA1 gene determines a second triglyceride synthetic pathway in yeast. *J. Biol. Chem*. 277:8877–8881. https://doi.org/10.1074/jbc.M111646200

Olzmann, J.A., and P. Carvalho. 2019. Dynamics and functions of lipid droplets. *Nat. Rev. Mol. Cell Biol*. 20:137–155. https://doi.org/10.1038/s41580-018-0085-z

Pascual, F., and G.M. Carman. 2013. Phosphatidate phosphatase, a key regulator of lipid homeostasis. *Biochim. Biophys. Acta*. 1831:514–522. https://doi.org/10.1016/j.bbalip.2012.08.006

Paul-Gilloteaux, P., X. Heiligenstein, M. Belle, M.C. Domart, B. Larijani, L. Collinson, G. Raposo, and J. Salamero. 2017. eC-CLEM: flexible multi-dimensional registration software for correlative microscopies. *Nat. Methods*. 14:102–103. https://doi.org/10.1038/nmeth.4170

Pédelacq, J.D., S. Cabantous, T. Tran, T.C. Terwilliger, and G.S. Waldo. 2006. Engineering and characterization of a superfolder green fluorescent protein. *Nat. Biotechnol*. 24:79–88. https://doi.org/10.1038/nbt1172

Salo, V.T., I. Belevich, S. Li, L. Karhinen, H. Vihinen, C. Vigouroux, J. Magré, C. Thiele, M. Hölttä-Vuori, E. Jokitalo, et al. 2016. Seipin regulates ER-lipid droplet contacts and cargo delivery. *EMBO J*. 35:2699–2716. https://doi.org/10.15252/embj.201695170

Salo, V.T., S. Li, H. Vihinen, M. Hölttä-Vuori, A. Szkalisity, P. Horvath, I. Belevich, J. Peränen, C. Thiele, P. Somerharju, et al. 2019. Seipin

Facilitates Triglyceride Flow to Lipid Droplet and Counteracts Droplet Ripening via Endoplasmic Reticulum Contact. *Dev. Cell*. 50:478–493. https://doi.org/10.1016/j.devcel.2019.05.016

Sandager, L., M.H. Gustavsson, U. Ståhl, A. Dahlqvist, E. Wiberg, A. Banas, M. Lenman, H. Ronne, and S. Stymne. 2002. Storage lipid synthesis is non-essential in yeast. *J. Biol. Chem*. 277:6478–6482. https://doi.org/10.1074/jbc.M109109200

Schorb, M., I. Haberbosch, W.J.H. Hagen, Y. Schwab, and D.N. Mastronarde. 2019. Software tools for automated transmission electron microscopy. *Nat. Methods*. 16:471–477. https://doi.org/10.1038/s41592-019-0396-9

Sorger, D., and G. Daum. 2002. Synthesis of triacylglycerols by the acyl-coenzyme A:diacyl-glycerol acyltransferase Dga1p in lipid particles of the yeast Saccharomyces cerevisiae. *J. Bacteriol*. 184:519–524. https://doi.org/10.1128/JB.184.2.519-524.2002

Szymanski, K.M., D. Binns, R. Bartz, N.V. Grishin, W.P. Li, A.K. Agarwal, A. Garg, R.G. Anderson, and J.M. Goodman. 2007. The lipodystrophy protein seipin is found at endoplasmic reticulum lipid droplet junctions and is important for droplet morphology. *Proc. Natl. Acad. Sci. USA*. 104: 20890–20895. https://doi.org/10.1073/pnas.0704154104

Thaller, D.J., M. Allegretti, S. Borah, P. Ronchi, M. Beck, and C.P. Lusk. 2019. An ESCRT-LEM protein surveillance system is poised to directly monitor the nuclear envelope and nuclear transport system. *eLife*. 8. e45284. https://doi.org/10.7554/eLife.45284

Vaden, D.L., V.M. Gohil, Z. Gu, and M.L. Greenberg. 2005. Separation of yeast phospholipids using one-dimensional thin-layer chromatography. *Anal. Biochem*. 338:162–164. https://doi.org/10.1016/j.ab.2004.11.020

Walther, T.C., J. Chung, and R.V. Farese, Jr.. 2017. Lipid Droplet Biogenesis. *Annu. Rev. Cell Dev. Biol*. 33:491–510. https://doi.org/10.1146/annurev-cellbio-100616-060608

Wang, H., M. Becuwe, B.E. Housden, C. Chitraju, A.J. Porras, M.M. Graham, X.N. Liu, A.R. Thiam, D.B. Savage, A.K. Agarwal, et al. 2016. Seipin is required for converting nascent to mature lipid droplets. *eLife*. 5. e16582. https://doi.org/10.7554/eLife.16582

Wang, S., F.Z. Idrissi, M. Hermansson, A. Grippa, C.S. Ejsing, and P. Carvalho. 2018. Seipin and the membrane-shaping protein Pex30 cooperate in organelle budding from the endoplasmic reticulum. *Nat. Commun*. 9: 2939. https://doi.org/10.1038/s41467-018-05278-2

Wolinski, H., H.F. Hofbauer, K. Hellauer, A. Cristobal-Sarramian, D. Kolb, M. Radulovic, O.L. Knittelfelder, G.N. Rechberger, and S.D. Kohlwein. 2015. Seipin is involved in the regulation of phosphatidic acid metabolism at a subdomain of the nuclear envelope in yeast. *Biochim. Biophys. Acta*. 1851: 1450–1464. https://doi.org/10.1016/j.bbalip.2015.08.003

Wu, H., P. Carvalho, and G.K. Voeltz. 2018. Here, there, and everywhere: The importance of ER membrane contact sites. *Science*. 361. eaan5835. https://doi.org/10.1126/science.aan5835
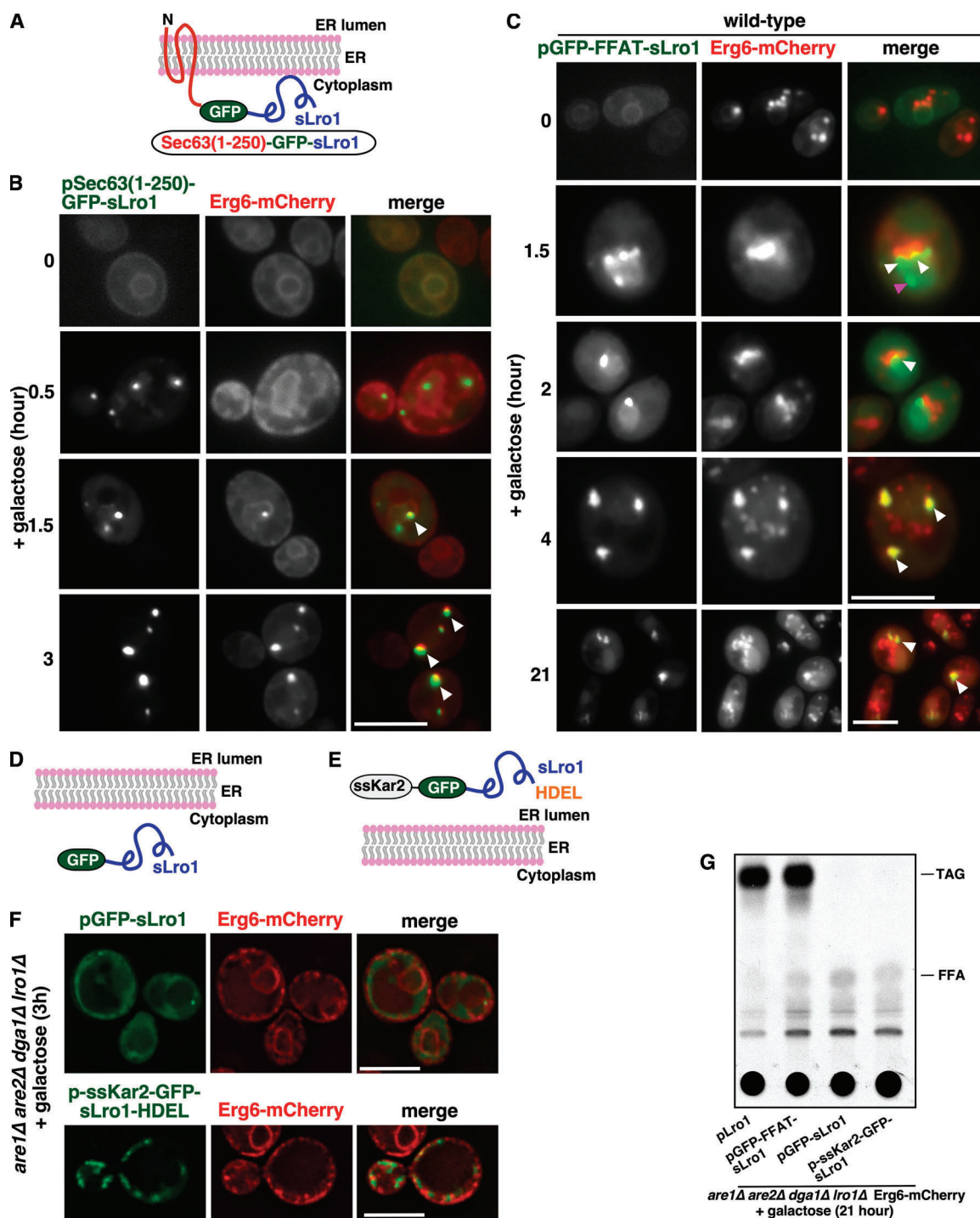
Supplemental material

Figure S1. **Data associated with Fig. 1.** TAG-synthase sLro1 needs to be ER associated for its activity. **(A and B)** sLro1-containing TMDs from Sec63 localize to ER subdomains. Design of the TAG-synthase chimera containing TMDs 1–3 from Sec63 (aa 1-250), facing the active site to the cytoplasm [Sec63(1–250)-GFP-sLro1] (A). 4ΔKO cells expressing Erg6-mCherry and coexpressing Sec63(1–250)-GFP-sLro1 from a galactose-inducible promoter were grown in raffinose media and switched to galactose media for the indicated period of time (B). White arrowheads indicate colocalization of Sec63(1–250)-GFP-sLro1 punctae with Erg6-mCherry. Scale bar, 5 μm. **(C)** GFP-FFAT-sLro1 localizes to LDs in WT cells. WT cells expressing Erg6-mCherry and coexpressing GFP-FFAT-sLro1 from a galactose-inducible promoter were grown as described in B. White arrowheads indicate colocalization of GFP-FFAT-sLro1 punctae with Erg6-mCherry. The pink arrowhead denotes a GFP-FFAT-sLro1 puncta not associated with Erg6-mCherry. Scale bars, 5 μm. **(D–F)** The TAG-synthase sLro1 needs to be anchored to the ER membrane for its activity. Design of the soluble fusion protein GFP-sLro1 localized in the cytosol (D), and ssKar2-GFP-sLro1-HDEL localized in the ER lumen (E). 4ΔKO cells expressing Erg6-mCherry and coexpressing either GFP-sLro1 or ssKar2-GFP-sLro1-HDEL from a galactose-inducible promoter. Cells were grown in raffinose media and switched to galactose-containing media for 3 h (F). Scale bars, 5 μm. **(G)** Nonmembrane-associated sLro1 fails to catalyze TAG synthesis. 4ΔKO cells expressing genomic Erg6-mCherry and coexpressing either native Lro1, GFP-FFAT-sLro1, GFP-sLro1, or ssKar2-GFP-sLro1-HDEL from a galactose-inducible promoter were grown in galactose media containing [³H]palmitic acid for 21 h. Lipids were extracted and separated by TLC. FFA, free fatty acid.
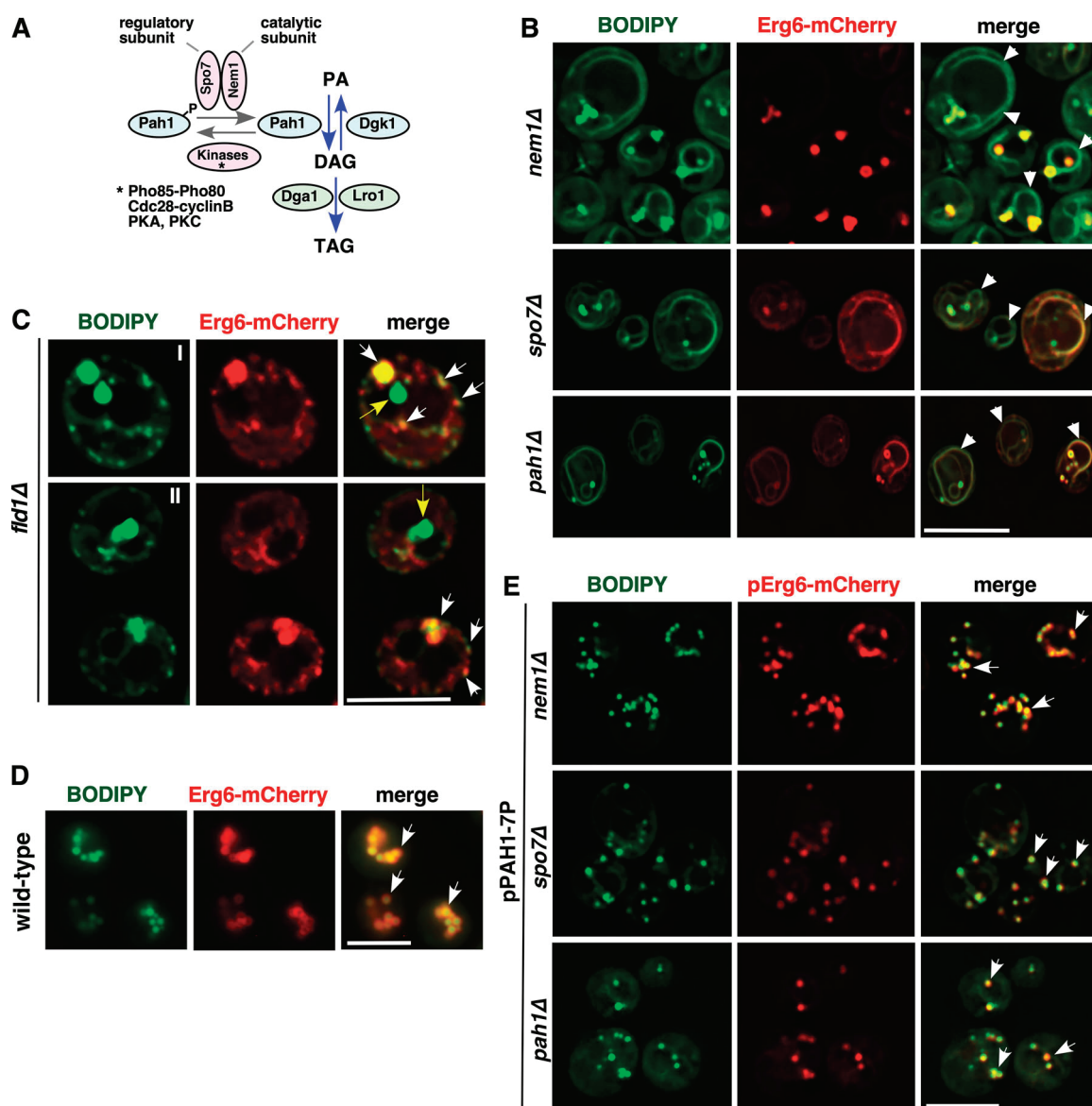
21

Figure S2. **Data associated with Fig. 2.** Cells lacking Nem1, Spo7, Pah1, or Fld1 accumulate neutral lipids in the ER and have aberrant droplets. **(A)** Diagram depicting the regulation of triglyceride synthesis. The Nem1-Spo7 complex dephosphorylates and thereby activates the phosphatidate phosphatase Pah1, resulting in formation of DAG from phosphatidic acid (PA). DAG then serves as a substrate for the TAG-synthesizing enzymes Dga1 and Lro1. **(B)** BODIPY accumulates in the ER of *nem1Δ*, *spo7Δ*, and *pah1Δ* cells. Yeast cells of the indicated genotype expressing genomic Erg6-mCherry were stained with BODIPY. White arrowheads denote BODIPY accumulation in the ER membrane. Scale bar, 5 μm. **(C)** Fld1-deleted cells accumulate numerous small and a few supersized LDs. *fld1Δ* cells expressing genomic Erg6-mCherry were stained with BODIPY. White arrows denote colocalization between BODIPY and Erg6-mCherry. Yellow arrows denote BODIPY-stained supersized puntae that do not colocalize with Erg6-mCherry. Two examples are shown (I, II). Scale bar, 5 μm. **(D)** WT cells do not show BODIPY accumulation in the ER. BODIPY staining of WT cells expressing genomic Erg6-mCherry. White arrows denote colocalization between BODIPY and Erg6-mCherry. Scale bar, 5 μm. **(E)** Pah1-7P rescues the LD biogenesis defect of *nem1Δ*, *spo7Δ*, and *pah1Δ* mutant cells. BODIPY staining of *nem1Δ*, *spo7Δ*, and *pah1Δ* mutants expressing Erg6-mCherry and Pah1-7P. White arrows denote colocalization between BODIPY and Erg6-mCherry. Scale bar, 5 μm.
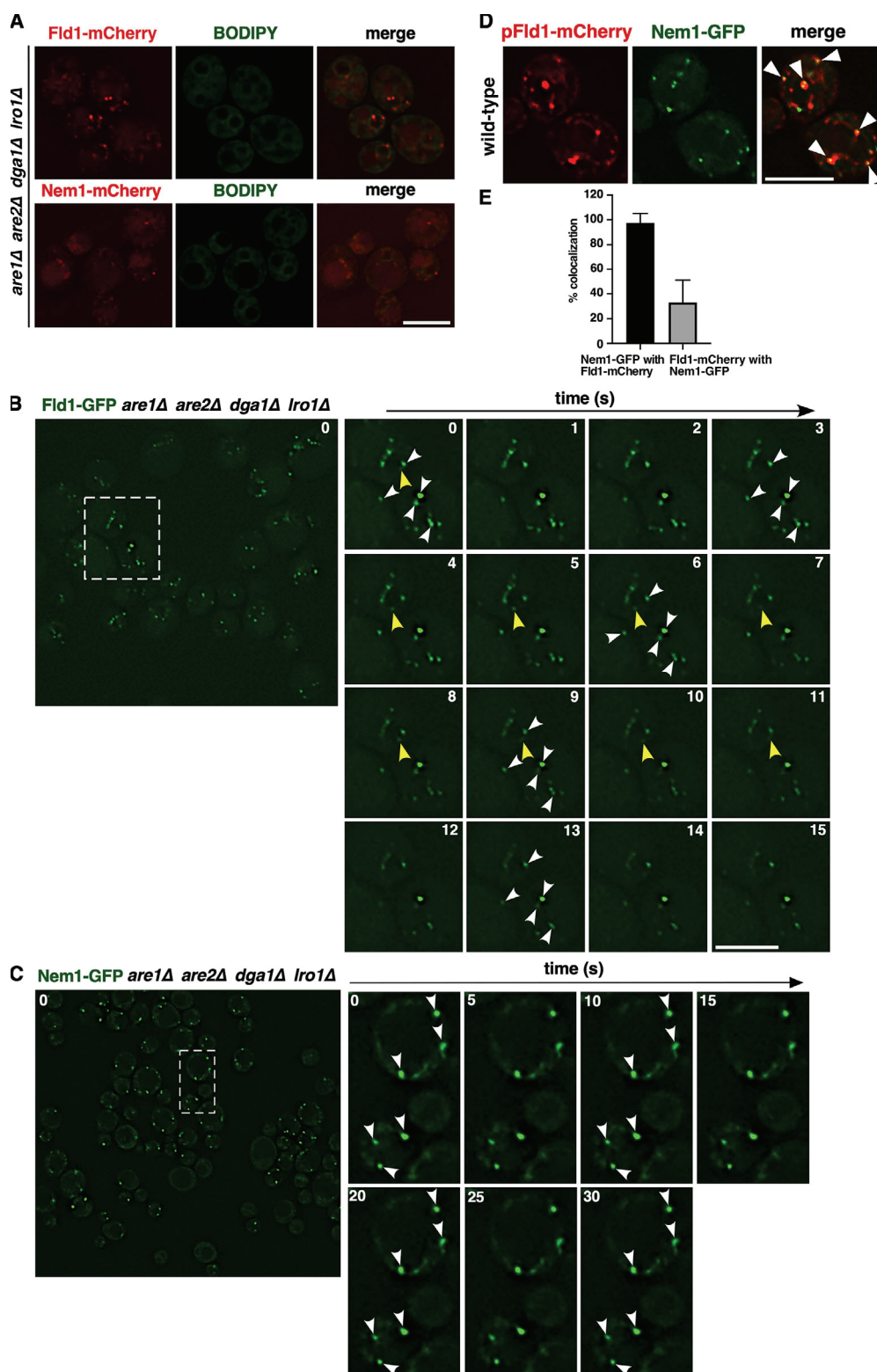
Figure S3. **Data associated with Figs. 2 and 3.** Fld1 and Nem1 localize to punctae in cells devoid of neutral lipids or LDs. **(A)** Localization of Fld1 or Nem1 to ER foci is independent of neutral lipid synthesis or the presence of LDs. BODIPY staining of 4ΔKO cells expressing genomic Fld1-mCherry or Nem1-mCherry. Scale bar, 5 μm. **(B and C)** Time-lapse images of Fld1-GFP and Nem1-GFP. 4ΔKO cells expressing genomic Fld1-GFP (B) or Nem1-GFP (C) were grown to early stationary phase, and time-lapse images were recorded. The boxed region in B and C is shown in higher magnification. Snapshots of images at the indicated time points are shown. White arrowheads indicate Fld1 or Nem1 punctae that stay immobile in the ER membrane. Yellow arrowheads denote rapidly moving Fld1 punctae. Scale bars, 5 μm. **(D)** Fld1 colocalizes with Nem1. WT cells expressing Nem1-GFP and coexpressing Fld1-mCherry were imaged. White arrowheads denote colocalization between Fld1 and Nem1. Scale bar, 5 μm. **(E)** Quantification of colocalization between Nem1-GFP and Fld1-mCherry. Data are means ± SD, *n* > 50 cells.
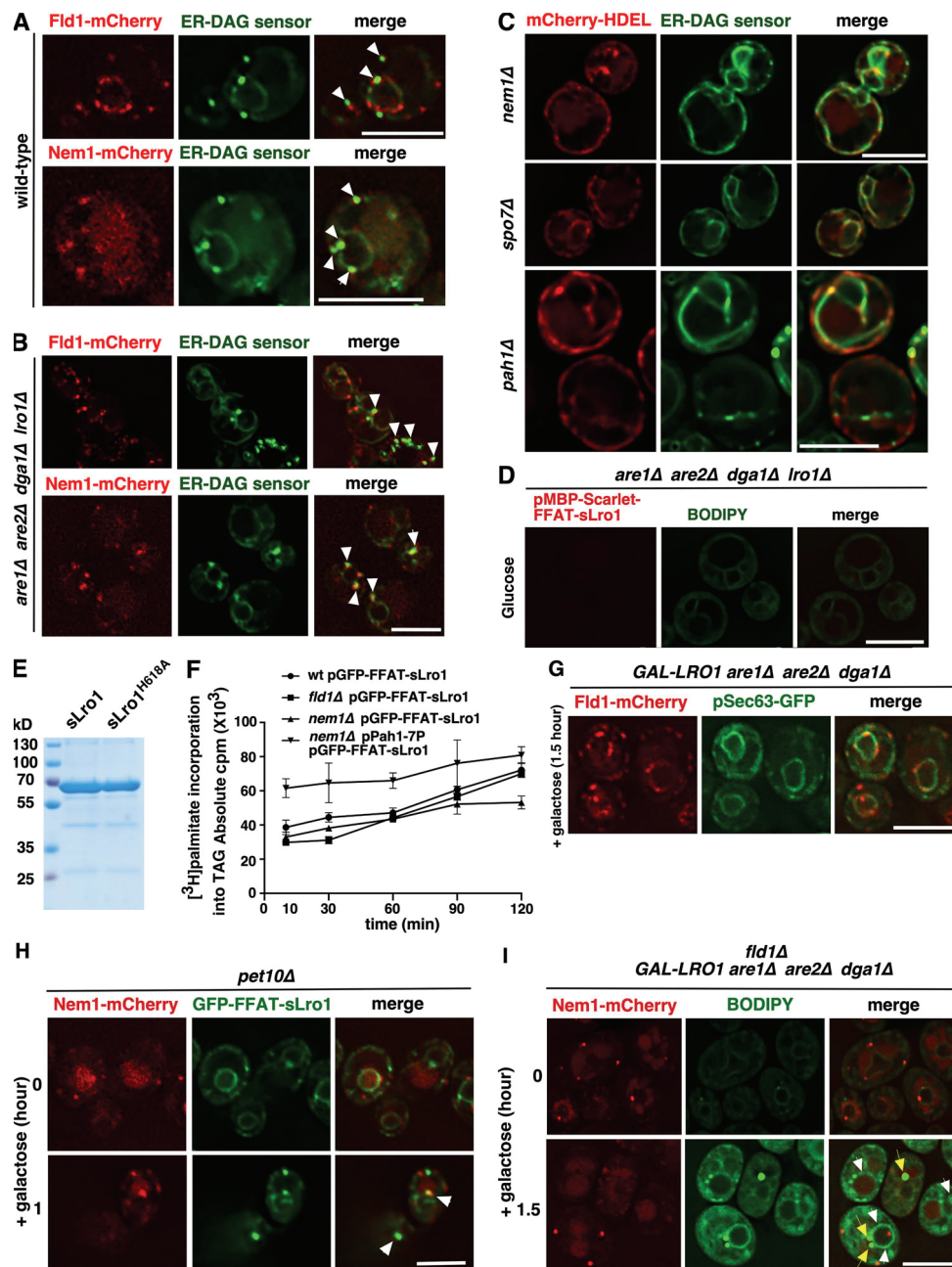
23

Figure S4. Data associated with Figs. 4, 5, 6, 7, and 8. Enrichment of DAG at Fld1 and Nem1 ER subdomains. **(A)** ER subdomains marked by Fld1 and Nem1 show enrichment of DAG. WT cells expressing Fld1-mCherry or Nem1-mCherry and coexpressing the GFP-tagged ER-DAG sensor were grown in SC media to early stationary phase and imaged live. White arrowheads indicate colocalization of the ER-DAG sensor with ER punctae marked with Fld1 or Nem1. Scale bars, 5 μm. **(B)** Fld1- and Nem1-marked ER subdomains show enrichment of DAG in LD-deficient cells. 4ΔKO cells expressing Fld1-mCherry or Nem1-mCherry and coexpressing the ER-DAG sensor were grown as described in A. White arrowheads indicate colocalization of the ER-DAG sensor with punctae marked by Fld1 or Nem1. Scale bar, 5 μm. **(C)** Lack of Nem1, Spo7, or Pah1 results in uniform distribution of the ER-DAG sensor. nem1Δ, spo7Δ, or pah1Δ mutant cells expressing the ER-DAG sensor were grown as described in A. ER was visualized by mCherry-HDEL. Scale bar, 5 μm. **(D)** BODIPY staining of 4ΔKO cells expressing MBP-Scarlet-FFAT-sLro1. Cells were grown in glucose media to mid-log phase. Scale bar, 5 μm. **(E)** Coomassie blue staining of an SDS-PAGE gel showing purified WT and mutant sLro1. **(F)** Rate of TAG synthesis. Time-dependent incorporation of [^{3}H]palmitic acid into TAG in the indicated yeast mutant cells. Cells were labeled and collected at 10-, 30-, 60-, 90-, and 120-min time points. Data are means ± SD of three independent experiments. **(G)** An ER membrane protein that is not involved in LD biogenesis does not show enrichment at Fld1-marked ER subdomains. The ER protein Sec63 does not become enriched at Fld1 sites during induction of LD biogenesis. GAL-LRO1 3ΔKO cells expressing Fld1-mCherry and coexpressing Sec63-GFP were grown in raffinose media and switched to galactose-containing media for 1.5 h. Scale bar, 5 μm. **(H)** Lack of Pet10 does not affect Nem1 localization and recruitment of TAG-synthase. The recruitment of GFP-FFAT-sLro1 to Nem1 sites is not affected in pet10Δ mutant cells. pet10Δ mutant cells expressing Nem1-mCherry and coexpressing GFP-FFAT-sLro1 from a galactose-inducible promoter were shifted to galactose media for the indicated period of time. Arrowheads denote colocalization of sLro1 with Nem1 foci. Scale bar, 5 μm. **(I)** Neutral lipids accumulate in the ER membrane in seipin mutant cells. fld1Δ mutant cells (fld1Δ GAL-LRO1 3ΔKO) expressing Nem1-mCherry were grown in raffinose media and transferred to galactose-containing media for the indicated period of time, stained with BODIPY, and imaged. White arrowheads indicate BODIPY accumulation in the ER. Yellow arrows indicate BODIPY punctae that do not colocalize with Nem1 foci. Scale bar, 5 μm.
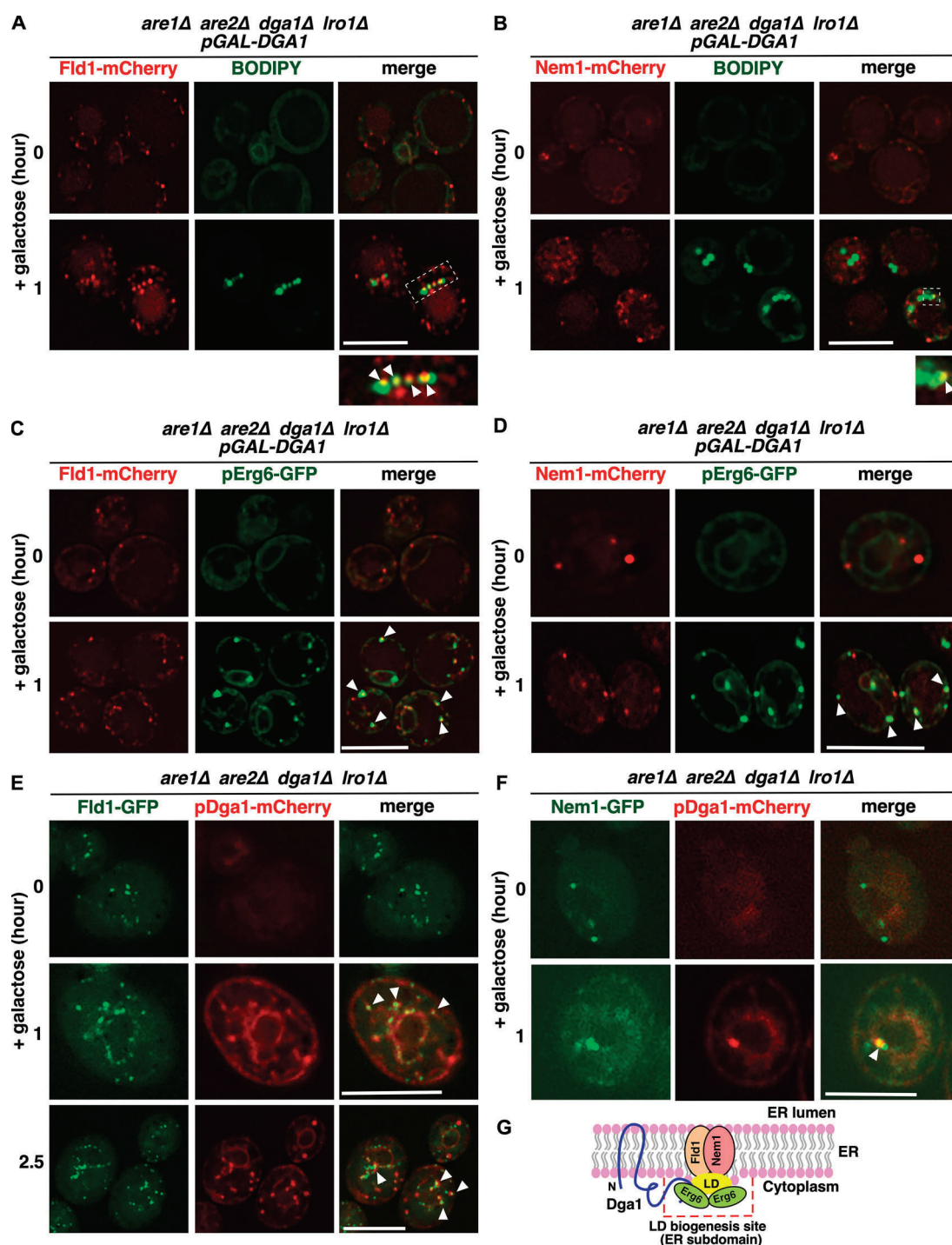
Figure S5. **Induction of TAG-synthase Dga1 results in LD formation at Fld1 and Nem1 sites. (A and B)** Fld1 and Nem1 sites are stained with BODIPY upon TAG synthesis. 4ΔKO cells expressing Fld1-mCherry (A) or Nem1-mCherry (B) and coexpressing Dga1 from a galactose-inducible promoter were switched to galactose media for 1 h and stained with BODIPY. White arrowheads indicate colocalization between BODIPY and Fld1/Nem1 punctae. Scale bars, 5 μm. **(C and D)** ER subdomains marked by Fld1 and Nem1 become enriched with LD marker protein. 4ΔKO cells expressing Fld1-mCherry (C) or Nem1-mCherry (D), Erg6-GFP, and coexpressing Dga1 from a galactose-inducible promoter were grown as described in A. White arrowheads indicate colocalization between Erg6 and Fld1/Nem1 punctae. Scale bars, 5 μm. **(E and F)** Dga1 colocalizes with Fld1/Nem1 sites. 4ΔKO cells expressing Fld1-GFP (E) or Nem1-GFP (F) and coexpressing Dga1-mCherry from a galactose-inducible promoter were switched to galactose for the indicated time. White arrowheads denote colocalization between Dga1-mCherry and Fld1-GFP/Nem1-GFP punctae. Scale bars, 5 μm. **(G)** Cartoon illustrating the recruitment of Dga1-mCherry to Fld1 and Nem1 ER sites, where droplets begin to form.

Video 1. **Data associated with Fig. S3 B.** Fld1-GFP localizes to ER subdomains independent of neutral lipid synthesis. Time-lapse images of 4ΔKO yeast cells expressing genomic Fld1-GFP. Stacks of seven images with a step size of 0.5 µm were acquired at an interval of 1 s for 15 s with an exposure of 500 ms, and deconvolved. Single plane images are displayed.

Video 2. **Data associated with Fig. S3 C.** Localization of Nem1-GFP at ER subdomains is independent of neutral lipid synthesis. Time-lapse images of yeast cells devoid of LDs (4ΔKO) expressing Nem1-GFP from genomic locus. Stacks of seven images with a step size of 0.5 µm were acquired at an interval of 1 s for 60 s with an exposure of 500 ms, and deconvolved. Images from a single plane are shown.

Video 3. **Data associated with Fig. 2 H.** Fld1-marked ER sites recruit TAG-synthase GFP-FFAT-sLro1. Time-lapse images of *fld1Δ* yeast cells overexpressing plasmid-borne Fld1-mCherry and coexpressing GFP-FFAT-sLro1 from a galactose-inducible promoter. Cells were shifted to galactose-containing media for 1 h. Stacks of seven images with a step size of 0.5 µm were acquired at an interval of 1 s for 30 s with an exposure of 500 ms, and deconvolved. Images from a single plane are shown.

Table S1 is provided online and lists *S. cerevisiae* strains and plasmids used in this study.